Accepted Manuscript

Journal of the Geological Society

The nature and significance of rift-related, near-surface fissure fill networks in fractured carbonates below regional unconformities

Kit Hardman, Robert E Holdsworth, Edward Dempsey & Ken McCaffrey

DOI: https://doi.org/10.1144/jgs2020-074

Received 23 April 2020
Revised 2 June 2020
Accepted 15 June 2020

Supplementary material at https://doi.org/10.6084/m9.figshare.c.5023103

The nature and significance of rift-related, near-surface fissure fill networks in fractured carbonates below regional unconformities

Kit Hardman[1,2], Robert E Holdsworth[1,3], Edward Dempsey[2], Ken McCaffrey[1,3]

1 = Department of Earth Sciences, Durham University, Durham DH1 3LE, UK
2 = Department of Geography, Environment and Earth Sciences, University of Hull, Hull HU6 7RX, UK
3 = Geospatial Research Ltd, Durham DH1 4EL, UK

Abstract: Hosted in carbonate and crystalline basement rocks below regional unconformities, fissure-fill networks are a widely recognized, but relatively little described near-surface phenomenon (<1-2km). Faults and fractures in otherwise tight Devonian carbonate basement rocks of the Tor Bay region, Devon, are associated with the development of millimetre- to decametre-wide fissures containing red early Permian sedimentary material, vuggy calcite mineralisation and wall-rock collapse breccias. These features preserve evidence concerning the style and history of fault deformation and reactivation in near surface settings, and on fluid-related processes such as elutriation and/or mineralization. Field observations, palaeostress analysis, and fracture topology analyses show that the rift-related faults and fractures created a network of long-lived open cavities during the early Permian development of the Portland-Wight Basin. Once formed, they were subjected to episodic, likely seismically-induced fluid fluxing events and local karstification. The large, well-connected networks of naturally propped fractures were - and possibly still are - important fluid migration pathways within otherwise low permeability host rocks. These structures are likely equivalent to those observed in many other rift-related, near-surface tectonic settings, and suggest that the Tor Bay outcrops can be used as a global analogue for sub-unconformity open fissure systems hosted in low permeability basement rocks.

Supplementary material: Appendix A is available at
https://doi.org/10.6084/m9.figshare.c.5023103

Cavern systems are widely developed across a range of scales in carbonate sequences worldwide and are known to be sustained as open features to depths greater than 2km due to the cohesion and relatively high tensile strength of most lithified limestones (e.g. Smart

et al. 1988; van Gent *et al.* 2010). Many modern examples are associated with younger sedimentary fills and low temperature carbonate mineralization. These features are known to strongly control present-day fluid flow pathways and processes and, more generally, the hydraulic behaviour of carbonates in the near subsurface (e.g. Popov *et al.* 2009).

Ancient and modern carbonate cavity systems are commonly referred to as 'karst' features and their formation mechanisms are typically attributed substantially to dissolution processes. However, very similar features are also recognised in other strong host rocks fractured in near surface environments (<1-2km depth), such as basalts (e.g. Angelier & Mechler 1977; Schlische & Ackermann 1995; Walker *et al.* 2011) and crystalline basement (e.g. Beacom *et al.* 1999; Siddoway & Gehrels 2014; Holdsworth *et al.* 2019). In most of these cases, solution processes are relatively minor or absent. Theoretical considerations and analogue modelling studies show that the relatively high strength of carbonate or crystalline rocks will tend to favour the formation of sub-vertical dilational fissures in the near surface during rift-related normal or strike-slip faulting episodes (Figs 1a-c; e.g. Sibson 1996; Ferrill & Morris 2003; van Gent *et al.* 2010; von Hagke *et al.* 2019). We should therefore expect such features to be widely preserved in ancient settings where fractured carbonates (or crystalline basement) form a basement that was exposed at the palaeosurface below regional erosional unconformities during the early stages of rifting, prior to burial. Given the frequent global development of hydrocarbon and geothermal reservoirs in fractured carbonates located close to regional erosional unconformities in the subsurface (Yang *et al.* 2014; Narayan *et al.* 2018), these fault-related fissure systems are likely to be of potential economic significance.

Massively dilated, ancient examples of carbonate-hosted fault zones are already known, for example the folded Tertiary carbonates in the UAE and Oman (van Gent *et al.*

2010), where they are filled with carbonate veins, fractured wall rocks and laminated sediment fills. Similar normal fault fissure fills – thought to be Triassic to early Jurassic age based on fossil evidence - are widely recognised in the fractured Carboniferous limestone basement that underlies the regional post-Variscan unconformity in the Bristol Channel Basin (e.g. Wall & Jenkyns 2004; Wright *et al.* 2009; Woodcock *et al*. 2014 - see their figure 13).

In this paper, we describe in detail the nature and significance of fissure systems filled with sedimentary material, breccia and calcite-dominated mineral deposits hosted in fractured Devonian limestones cropping out on the western onshore flanks of the offshore Portland-Wight Basin in Torbay, SW England (Fig. 2). We examine the diverse architecture of these fissure fills and their associations with rift-related normal faults, the nature and mechanisms of filling and discuss the significance of our findings for fluid flow and fluid reservoir development in the subsurface.

Geological setting

Regional context and stratigraphy

Tor Bay in SW England lies within the English Riviera UNESCO Global Geopark, stretching 9 km from Hope's Nose (SX 94741 63546) southwards to Berry Head (SX 94563 56538) (Fig. 2). A structurally complex *basement* sequence of Devonian limestones and calcareous mudstones was deformed by during the Variscan Orogeny (Coward & McClay 1983). It includes, from oldest to youngest: the Early Devonian Meadfoot Group; Middle Devonian Nordon Formation; Brixham (or Torbay) Limestone Formation; and Late Devonian Saltern

Cove Formation (Strange 2001). Devonian basaltic tuffs and intrusive dolerites occur at Saltern Cove, Black Head, and Oddicombe Beach (Fig. 2) (Ussher 1903).

A little deformed and shallowly dipping (<10^{o}) *cover* sequence of red, early Permian sandstones and breccias outcrops mainly within the central part of the Tor Bay coast (Fig. 2) (George *et al.* 1927; Shannon 1928; Strange 2001). These rocks belong to the Torbay Breccia Formation, part of the Exeter Group (Ussher 1903; Henson 1971). They form a well-bedded sedimentary succession, starting with alluvial conglomerates and depositional breccias at the base, before sharply transitioning to younger cross-bedded and well sorted aeolian sandstones. The basement and cover are separated by a regional-scale, post-Variscan erosive angular unconformity known locally as the 'Goodrington Unconformity' (best exposed at SX 89539 58742).

Extensive outcrops of Permo-Triassic and Jurassic sandstones occur along the South Devon-Dorset coastline to the east of Tor Bay, which also form key potential reservoir rocks in the offshore SW Approaches petroleum system (Shail & Leveridge 2009 and references therein). Though separated by the NW-SE trending Stickleback-Lustleigh fault zone, the Tor Bay area lies on the western flanks of the offshore Portland-Wight Basin (Fig. 2; Harvey *et al.* 1994; Underhill & Stoneley 1998). The form of the Tor Bay coastline and margins of the offshore basin are significantly controlled by regional-scale, sub-vertical fault zones.

Pleistocene karst systems are widely developed in the Devonian limestones onshore (e.g. Kent's Cavern; Ussher 1903; Lundberg & McFarlane 2007), together with interglacial raised beach sediments (Strange 2001; Leveridge & Hartley 2003).

Structural Evolution

During the Variscan Orogeny, northward-directed contractional deformation led to the development of northward verging minor folds, cleavages and thrust faults in the Devonian

basement sequences (e.g. see Coward & McClay 1983). Following uplift, exhumation and regional erosion, the exposed limestone basement around Torbay experienced one or more phases of extensional tectonics, subsidence and sedimentation leading to the formation of large, steeply-dipping to sub-vertical NNE-SSW and E-W to ENE-WSW faults and the regional-scale Goodrington Unconformity (Harvey *et al.* 1994; Shail & Wilkinson 1994) (Fig. 2). Permian extension here is thought to be related to post-orogenic collapse of the uplifted Variscan orogenic belt (Harvey *et al.* 1994; Ruffell & Shelton 2000). Some large basin-bounding faults are seen onshore (e.g. at Crystal and Saltern coves), whilst others are inferred to lie just offshore with smaller fracture arrays occurring in aligned swarms and corridors throughout Tor Bay (Fig. 2). Open fissures associated with both fracture sets are known to be filled with zoned calcites, complex breccias, and significant volumes of red sedimentary material (e.g. Richter 1966).

Following a period of tectonic quiescence in the Triassic, active rifting resumed during the Jurassic. This extension was centred offshore to the E of Tor Bay, generating large sedimentary depocentres off the Dorset coast in the Portland-Wight Basin (Underhill & Stoneley 1998). Unequivocal evidence for this phase of extension is not observed within the study area as there are no exposed Jurassic rocks onshore, but it is clearly seen offshore in seismic reflection profiles (e.g. see Underhill & Stoneley 1998).

A later Cenozoic disconformity occurs in the Eocene-Oligocene strata of southern Britain and reflects a further period of regional uplift. At around this time, several kilometres of sinistral strike slip motion are thought to have occurred along the regional NW-SE Sticklepath-Lustleigh Fault Zone (Fig. 2; Holloway & Chadwick 1986). This NW-SE fault zone presently separates the onshore Tor Bay area from the offshore Portland-Wight Basin located further to the E (Fig. 2).

Field and laboratory methods

Fractures systems and their fills were studied at 14 localities around Tor Bay (Fig. 2) where they are well exposed in the Devonian carbonate basement located close to the Goodrington Unconformity in coastal cliffs, wave-cut platforms, and quarries (Fig. 2). Structural geometries were recorded through the collection of orientation data, with brittle fault kinematics measured from: offsets of markers in the host rocks, the local preservation of slickenline lineations, and the preservation of asymmetric shear criteria such as en-echelon veins and slickenline steps (Petit 1987). The relative ages of fractures and their associated fills were ascertained in the field from observation of cross-cutting relationships. In exceptionally well exposed cliff sections and rock platforms, observations and interpretations were also made using low-level areal images collected using a drone. Representative samples of oriented hand specimens were collected from mineral and sediment fills of fractures and were used to study the microstructure and relative-age relationships of mineralization and cementation using transmitted light optical microscopy.

As many of the fracture systems studied include faults with slickenline lineations, we used palaeostress inversion techniques to determine an approximation of the stress conditions responsible for their formation. This was carried out using WinTensor software (Delvaux & Sperner 2003), which utilises both the PBT axes method and the improved Right Dihedron method of Angelier & Mechler (1977) and Delvaux *et al.* (1995). These techniques have a consistent assumption that the slip vector data recorded in the field is parallel to the ideal shear component of the resolved stress tensor (Wallace 1951; Bott 1959). They are most appropriate where the host rock is mechanically isotropic, fault displacements are

small, and where data is measured across a broad range of fault plane orientations (Angelier 1991).

In order to quantify fracture connectivity and volume of sediment fills in the Devonian basement, a drone-based orthorectified virtual outcrop model (VOM) was created for one very well exposed rock platform at Shoalstone Beach (Fig. 2) with an effective viewing resolution of 1-2cm. This was then interpreted manually and "ground-truthed" during subsequent fieldwork, to generate a fracture trace map which was used to quantify fracture attributes, both manually and using the FracPaQ MatLab extension (Healy *et al.* 2017). The relative connectivity of the fracture network was determined using fracture topology (for details see Sanderson & Nixon 2015), a characterisation technique that simplifies a 2D fault or fracture network into discrete branches and nodes. The ratios between different types of nodes (I-Y or Y-X), and branches can be used to determine the relative connectivity and spatial characteristics of the network. In addition, areal and volumetric calculations of the amounts of fracture fills were undertaken using the Image Processing toolbox of MatLab (see Supplementary Material).

Post-Variscan fracture architectures and geological associations

Brittle fractures are well-preserved, cross-cutting Devonian basement rocks and the lowermost parts (<5m above basement) of Permian cover sequences around Tor Bay. These structures are characteristically highly dilational in character and comprise three distinct void-like forms described below.

Sub-vertical forms

Steeply-dipping to sub-vertical structures are the dominant form around Tor Bay. Two categories occur – *large normal faults* with apertures of up to 40m; and 10-100m wide

fracture corridors made up of fractures that individually have apertures of <1m. Note that throughout this paper, we use the term 'aperture' to refer to the width of a fracture including any fill, i.e. the '*kinematic aperture'* of Ortega *et al.* (2006).

Large normal faults

At Crystal Cove (SX 89656 58057) a 400m coastal section on the north side of Broadsands Beach exposes a linked array of three major, sub-vertical NNE-SSW faults with apertures up to 40m wide (Figs 3a-c). Red clastic sedimentary material intercalated with extensive vuggy calcite mineralisation fills the fault fissures (Figs 3c,e,f). A series of discrete slip surfaces with calcite slickenfibres (e.g. Fig. 3d) are recognised separating panels of sediment infill, brecciated basement wall rocks and dilatant calcite mineral fills (Fig 3b-f). Slickenfibres display normal dextral shear senses, with rakes varying from 63° to 90°, along planes which strike from 003° - 043° and dip 68° to 86° E (Fig. 3g). The aforementioned sediment fills are distinctly zoned, with each widening (increasing in aperture) towards the overlying palaeosurface unconformity in a "v" shape (e.g. Fig. 3c). These features likely formed as filled fissure cavities, each zone representing an individual dilatant opening event of the fissure. With each movement, the cavity widens creating new spaces that were infilled by sediment and/or by minerals precipitated from circulating hydrothermal or meteoric fluids. The repeated overprinting slickenfibres and zoned fills suggest repeated reactivation with synchronous shear and tensile fracturing behaviour close to the surface represented by the immediately adjacent base-Permian unconformity.

Some 200m north of Crystal Cove, a small inlet called Shell Cove (Fig. 3a; SX 89643 58217) preserves the unconformable contact between the Devonian limestone basement and the Permian clast-supported breccia and interbedded sandstone cover. The lowermost layers of this cover sequence are interpreted as flash-flood deposits and contain clasts of

the underlying limestone basement (Thomas 1909; Henson 1971). Sub-vertical NNE-SSW trending sandstone and breccia-filled fractures are seen to cut *both* the limestone basement and the lowest 2-3m of the overlying breccia. These rocks are then disconformably overlain by cross-bedded, finely laminated sandstone. It is difficult to demonstrate conclusively that the sedimentary material filling the fracture cavity is continuous with these Permian sandstones, but the lithologies are identical in composition, grain-size and rounding. We therefore suggest that the cross-bedded sandstone either forms the sediment source, or immediately post-dates the sediment fills in the underlying fractures and that both were deposited under similar environmental conditions.

E-W major faults are best observed at Oddicombe Beach (SX 92645 66127) and Saltern Cove (SX 89543 58377) (Figs 2, 4). In the latter locality, a large E-W trending fault system is observed in the cliffs with an aperture of 14m, dipping steeply N (Fig 4a, b). It cross-cuts a small, S-dipping Variscan thrust that emplaces Brixham Limestone Formation over rocks of the younger Saltern Cove Formation. The limestone hangingwall of the thrust fault has undergone dissolution at the intersection between the thrust and normal fault. Calcite-bearing vugs (c. 2-15cm) have developed here (Fig. 4f), some of which have been filled geopetally by well-bedded red sandstone. A large limestone clast lies suspended in a matrix of zoned, sub-horizontally bedded red sandstones (Fig. 4a, c) suggesting that emplacement of the block was contemporaneous with red sediment infilling; it appears to have fallen downwards into the cavity from the hangingwall of the pre-existing thrust. The infilled cavity also contains entrained volcanic material (Figs 4d, e).

Dilatant fault and fracture corridors

Sub-parallel corridors 10's to 100's of metres wide are best exposed in plan view at Shoalstone Beach, and in cross section at Berry Head Quarry (Fig. 2; Richter 1966; Wall &

Jenkyns 2004; Woodcock *et al.* 2014). Other important, though less well-developed examples occur at Hope's Nose. These fractures typically have apertures of 5-15cm, but have been observed as narrow as a few millimetres and as wide as 4.5m.

At Berry Head Quarry (SX 94293 56615) (Fig. 5a), the excavated Middle Devonian limestone walls are up to 60m high, with a single shelf exposure of cliff section 9km long. 26 sub-vertical sediment-filled fractures trending either NNE-SSW or ENE-WSW are seen here cutting homogenous massive limestones. No filled fissure tips are observed, with fractures extending vertically over many tens of metres with little systematic change in aperture. Despite having seemingly constant apertures over vertical distances of up to 60m, the walls of the fracture cavities are locally irregular, with many large angular asperities and entrained blocks of brecciated wall-rocks (Figs 5b-d). These features, together with the lack of any noticeable lateral offset of bedding in the surrounding limestones indicates that these are predominantly tensile (Mode I) opening fractures. At the western end of the quarry, a number of moderately dipping (~40^{o}) sediment-filled cavities are also exposed linking into vertical fractures ("low angle linkages" in Fig. 5d).

At the seafront quay, some 150m N of the main quarry, 5 bifurcating and linked, sediment-filled fractures occur with apertures up to 40cm (Figs 5a – yellow box, e, f). By tracing these fractures along strike to the equivalent set seen in the quarry walls, we can infer that these fractures are at least 500m long, and show little evidence of narrowing or tipping out laterally, indicating a still larger fracture trace-length. A minority of the exposed margins of these fractures appear to have been smoothed. These are interpreted as possible local karst weathering features (Dubois *et al.* 2014). This suggests that these cavities were open close the surface and permeable to fluids prior to infilling. Note, however, that the evidence for dissolution is generally very limited and the vast majority of exposed fracture

walls feature angular – sub-angular asperities that can be matched exactly to opposing fault walls, along with textures such as jigsaw brecciation, that would not be preserved had dissolution have widely affected the fracture surfaces.

A large wave-cut platform 700m long occurs at Shoalstone Beach, NE of Brixham harbour (SX 93608 56816) (Figs 2, 6; Richter 1966). Here an exceptional 2D plan view of sediment-filled fracture networks is exposed cutting Middle Devonian limestones (Figs 6a-h). As in previous locations, shear offsets of bedding are minimal and the fractures are almost entirely dilational Mode I features. Previous authors have noted that the sub-vertical fissures here occur in two sets (Richter 1966). An older, paler coloured ENE-WSW set is cross-cut by younger, darker N-S set (Figs F-H). These relative age relationships are typical of the Tor Bay region as a whole and, given the exceptional exposure, this locality can be regarded as the "type" locality for these sediment-filled fractures.

At Hope's Nose, Middle Devonian reef limestones are cut by irregular sediment- and calcite-filled faults and rare sulphide mineralised fault breccias (Figs 7a, b). Several faults exhibit a stratigraphic control where the mode of failure changes within different host units (e.g. Figs 7c, d). For example, where thicker bedded, more competent limestones are offset, the fault is dilatant (Mode I) with a wide aperture (up to 65cm) filled with sediment. Traced upwards into the directly overlying finer bedded limestones and tuffs, the fault shallows in dip by 20^{o} and becomes a narrower shear fracture (Mode II/III) (Fig. 7c). This section of the fault contains breccia and slickenlines which indicate a normal shear sense (Fig. 7e). In some cases, blind faults are observed to have generated open 'forced folds' directly above the propagating fault tip (Fig. 7d). The fracture sets at Hope's Nose exhibit cross cutting relationships opposite to those seen in the rest of Tor Bay, i.e. sets of (unfilled) N-S fractures here are cut by (sediment- and breccia-filled) E-W faults. These E-W structures show

brecciation of mineral fills suggesting that there was later local fault reactivation here which may help explain the difference in percolating fluid chemistries at Hope's Nose described by Shepard *et al.* (2005). Once again, a minority of fractures at Hope's Nose exhibit smoothing of cavity walls and apparent locally widened apertures (e.g. Fig. 7a), suggesting some minor karstification prior to sediment infilling.

Sub-horizontal forms

Where present, sub-horizontal fracture cavities are usually associated with large vertical faults and fractures. They have previously been referred to as "Liassic veins", and "sedimentary sills" (Peterson 1967; Richter 1966; Smith 1952). At Fishcombe Point (SX 91843 57053) (Figs 8a-d), two small horizontal, partially sediment-filled cavities occur in Middle Devonian limestone with exceptionally well-developed fractal-scalenohedral calcite crystals which line the cavity walls (Figs 8c-f). These horizontal cavities link into a large (3-17cm wide, >10m long) vertical sediment-filled fracture, progressively thinning away from it until they eventually pinch out (Fig. 8c). The horizontal cavities are partially filled by a red homogenous sediment continuous with the sediment fills in the vertical fractures, although it is much finer grained (20-50µm versus 250-1000µm) (Figs 8d-f). These horizontal cavities are sub-parallel to the pre-existing bedding in the limestone basement (Fig. 8c) and feature locally smoothed cavity walls, indicating that some minor dissolution has occurred during cavity creation (Dubois *et al.* 2014).

Irregular cavity forms

Cavernous carbonate-hosted voids are subordinate features compared to the other forms of fill and are morphologically diverse. At Fishcombe Cove (SX 91979 56942) (Fig. 2), the coastal exposures host a densely packed network of steeply-dipping, sediment-filled fractures trending NNE-SSW and E-W (Figs 8b, i), which exhibit the same cross-cutting

relationships as seen at Shoalstone Beach. Less than 10m E along the coast, a near spherical fracture cavity up to 2m in diameter occurs filled with homogenous, un-bedded Permian sandstone. At Fishcombe Point, a series of small 20cm wide sediment-filled fractures are connected to a number of irregular lozenge-shaped, low aspect ratio (cave-like) cavities (1.7 x 0.5m), lined with calcite (c. 10cm thick) and filled with bedded Permian sandstone (Figs 8g, h).

Infills: nature and processes

The intimately associated sediment- and calcite-fills found associate with faults and fractures in the Tor Bay are must have formed close to the surface based on their proximity to the regional unconformity and the close lithological similarity of the sediment fills to the immediately overlying basal Permian strata.

Mineral fills

Fracture walls are typically lined by sparry calcite fills, which vary significantly in size and morphology from millimetre-thick blocky to metre-thick coarse crystalline spars (Figs 5e, 8d, f, 9a-g). Where sediment fills are present, the veins are normally a few centimetres thick and typically occupy < 10-15% of the fracture volume. The calcites are mostly milky white, but dark-grey fills are locally developed containing impurities such as carbon or fine iron oxide. Thick sparry calcite veins are consistently syntaxial and grow inward from the cavity walls (Figs 9a-f). Associated sediment fills are commonly cross-cut by smaller, younger calcite veins (e.g. Fig. 10b) and new fissure cavities may be present in the infilling sandstone which are also lined by crystalline calcite (e.g. Figs 3c, f).

A variety of crystalline calcite forms are observed (Fig. 9) including: scalenohedral (dog-tooth spar) (Fig. 9a) a delicate fractal scalenohedral variety (Fig. 9b); rhombohedral

(nail-head spar) (Fig. 9c); fine grained and sheeted (Fig. 9g); dendritic (Fig. 9e); mm-cm scale stalactites, and blocky calcite (Fig. 9d). Fibrous forms are largely absent except as slickenfibres developed on larger fault surfaces (e.g. Fig. 3d).

Syntaxial "cavity filling" textures are best displayed by the scalenohedral and rhombohedral forms (Figs 4f, 8d, f-h, 9a-f, 10b). Both types are known to form in near-surface environments (e.g. García Carmona *et al.* 2003; Milodowski *et al.* 2018) and the lack of mixed calcite morphologies in single fractures suggests that fluid compositions, water depth and/or temperature may have fluctuated during fissure filling.

Small amounts (<1cm thick) of fine and sheeted calcite – interpreted to be travertine and flowstone - are seen lining cavity walls in a minority of locations, e.g. Hope's Nose, Fishcombe Point (Fig. 9g). These features suggest that a limited degree of karstification may have affected some of the open fractures, which also show evidence for minor dissolution ('smoothing') along the cavity walls. These karstified fractures can be distinguished from the effects of later Cenozoic-Recent weathering as they are partially covered by Permian sandstone infills.

Calcite textures are consistently growth zoned with large scalenohedral calcites commonly showing orange bands, parallel to crystal faces (e.g. Fig. 9f). Colour zonations like this are thought to be controlled by small fluctuations in fluid conditions/chemistry (e.g. Fig. 13b) (Paquette *et al.* 1993; Guoyi Dong *et al.* 1995; Milodowski *et al.* 2018). The bright orange stained zones/bands within the calcite crystals likely formed due to enrichment of iron oxides in the mineralising fluids, which were then precipitated as thin haematite coatings and trapped as Fe-rich fluid inclusions (Milodowski *et al.* 2018). More generally, the syntaxial calcites show a marked coarsening-inward texture (Figs 9a-f, 10b). Multiple sequences of calcite growth from a single wall-rock interface are locally developed, with up

to three or four bands of coarsening-inward calcite within a single vein (e.g. Fig. 10b). This is likely due to repeated pulsing of fluids through the open fracture systems, each generating a renewed phase of mineralisation.

Sedimentary fills

Most fills in sub-vertical faults and fractures are consolidated red sandstones comprising well rounded, medium to coarse grains (200-100µm) of quartz coated in a thin layer of hematite (Figs 10a-e; Richter 1966). The grains are exceptionally well sorted, and most sands are homogeneous, structureless and massive (Figs 10d, e). Bedding, where present, is defined by small variations in grain size and/or by thin laminations of fine silt (Figs 3e, 4c, 5e, 6f, 8h). A proportion of the original porosity in the sediment fills is occluded by mineral cement, but open porosities of up to 10% are commonplace (e.g. Fig. 10c), and locally reach 35%.

In most of the Tor Bay area, fills in the older E-W set of fissures are calcite cemented, with a great deal of associated calcite veining, whereas fills in the younger N-S set also feature regions of quartz cement, in addition to lesser amounts of calcite (Richter 1966). It is not certain whether this reflects a change in depositional conditions, but in every other respect, the fissures are identical. Where calcite cements are present in sediment, they grow in optical continuity with large calcite crystals in adjacent mineral fills (Fig. 10a). Where quartz cements are present in the sediment fills of N-S fractures, they are seen to grow in optical continuity with the clastic quartz grains they enclose (Figs 10f, g), which can be recognised by a thin coating of haematite. Collectively, all of these features suggest that fissure-hosted sedimentation, cementation and calcite mineralization were all contemporaneous.

Further evidence for this contemporaneity comes from the preservation of striking pyramidal piles of sandstone-siltstone within large vertical fault fills and fractures (Fig. 3e). At Crystal Cove, hundreds of these red sediment pyramids can be seen in cross-section within a large calcite-lined N-S fault cavity. They vary in size from millimetres to tens of centimetres across, and in many places preserve shallowly-dipping bedding laminations in the centre of the pyramid, progressively steepening towards the margins (Fig. 3e). Similar features have been described by Woodcock *et al.* (2014) and are thought to represent geopetal accumulations of sediment which have been washed into open, partially mineralized fault cavities and piled up on any asperities or fallen clasts of wall-rock.

Chaotic breccia fills up to several metres wide are found in many sediment-filled fissures around Tor Bay. The most common type consists of irregularly orientated, angular clasts of wall-rock limestone that show no evidence for attrition or rounding (e.g. Figs 4a, c, 7b, 11c). These are thought to have formed by wall-rock collapse into open fissures (Woodcock *et al.* 2014). Locally, jigsaw-type breccias are developed where clast fragments are seen only slightly displaced from their original position (e.g. Fig. 5b). In all cases, the breccia clasts are held in a uniform matrix of red sandstone, suggesting that brecciation occurs coevally with sediment infilling.

A few more exotic fills are found locally in some larger fracture systems. At Saltern Cove, an irregular zone of breccia fill includes clasts of tephra with associated copper and lead mineralization, enclosed in a matrix of fine-grained red sandstone (Figs 4d, e). Clasts are of orange-coloured tuff, and copper-rich clasts of volcanic ejecta. The sandstone matrix here preserves bedding laminations that wrap around the volcaniclastic clasts, suggesting that they were already lithified before being incorporated into an open cavity along with the unlithified sand. This volcanic material may have originated from the Late Devonian

interstitial basaltic tuffs within the Saltern Cove Formation, reworked at the surface and emplaced into the cavity (Smith 1952). The vertical and horizontal zonation of the sediment infilling the large normal fault cavity here further suggests that this fault-related fissure was repeatedly and cyclically reactivated, dilating and filling iteratively over time.

At Fishcombe Point and SE of Fishcombe Cove, sedimentary fills in sub-horizontal fractures are finer grained (20-50μm) relative to adjacent vertical fracture fills and show normal grading consistent with deposition from a fluid suspension. This may indicate that these open fractures were regions of lower energy fluid flow, where finer sedimentary material elutriated from the adjacent, faster flowing vertical fracture cavities was deposited (Cox & Munroe 2016). The local development of sand volcanoes close to the intersections of vertical and horizontal cavities (e.g. Fig 8e) also points to fluid fluxing and elutriation. Along the slopes of the sand-volcanoes, interfingering sedimentary structures with slight variations in grain-size reveal different depositional events, showing that these likely formed iteratively over many repeated fluid flux events (Fig. 8e).

Finally, along the eastern side of Fishcombe Cove, a large lozenge-shaped sediment fill with an aperture of a few 10s of cm occurs (Figs 8g-i). The fracture is lined by sparry calcite, and the infilling sediment hosts an array of sedimentary structures including cross bedding and dewatering structures (Fig. 8h). Unusually, the earliest sediment fills here were concentrated along the sides of the cavity in very steep beds, most likely caught against the walls as the majority of the sediment fell deeper into the fault cavity. Once the steep beds met and blocked the fissure, shallowly dipping beds were deposited on top which preserve dewatering and flame structures consistent with periodic fluid fluxing events (Fig. 8h).

Discussion

Our observations indicate that the fracture-hosted cavities in Devonian Limestone basement are fault-related fissures formed at, or within no more than a few hundred metres of the surface that have been pervasively infilled by Permian red sediment, with broadly contemporaneous calcite (and minor quartz) mineralization. The near surface interpretation is predicated on the close spatial association between the occurrence of the red sediment fills and the presence of the regional (early Permian) unconformity. The clastic material either fell, or was washed, into a network of long-lived open, subterranean cavities and was then variably reworked and redistributed by periodic upward-directed fluid fluxes (Fig. 11). The intimate association between the sediment fills and the calcite-dominated mineral fills suggests that these fluid fluxes are plausibly related to active rifting in the early development of the Portland-Wight Basin.

Karstification vs tectonic fissure formation

Karstification plays a significant role in the development of cavity systems in shallow basement carbonates world-wide (Hauselmann *et al.* 1999). In the Tor Bay area, large Quaternary cave systems are known within the carbonate basement, such as Kent's Cavern (Lundberg & McFarlane 2007). However, most of the fracture cavities directly associated with Permian sediment and mineral fills in fissured limestone show very angular cavity walls and asperities with little or no evidence for aperture widening and dissolution (see also examples discussed by Woodcock *et al.* 2014). The preservation of faults with shear offsets and slickenlines is further evidence for tectonic faulting at the time of open fissure formation. Fifty slickenside lineation measurements and relative displacement senses were subjected to a stress inversion analysis. (Fig. 12). The results suggest that both E-W and N-S structures formed under an extensional radial stress system (vertical $\sigma 1$) with a NNW-SSE primary extensional axis ($\sigma 3$), and an ENE-WSW secondary extensional axis ($\sigma 2$) (Fig. 12).

Collectively these observations suggest that the majority of fissure fills here are of tectonic origin, and the extensional stress system demonstrates that they are most likely related to the early stages of Permian rifting and basin formation rather than Variscan contractional deformation. Analogue models of dilatant normal fault systems in carbonates have shown how vertical tensile fissures formed in the near surface link at depth to inclined hybrid and shear fractures with dilational jogs at intermediate levels (Figs 1a, b; van Gent *et al.* 2010). Importantly, the NNW-SSE extension direction derived here is consistent with the direction of Permian rifting inferred from onshore and offshore geological studies in SW England (see Shail & Leveridge 2009 and references therein).

Mineral filling mechanisms

Mineral zonation and cockade textures (Frenzel & Woodcock 2014; and references therein) are widely recognised on micro- to meso-scales, with the best examples preserved at Crystal Cove, Petit Tor Point, and Shoalstone Beach. Here the mineralized fracture cavity fills have individual clasts that are completely surrounded by, and therefore appear to float in, multiple concentric layers of cement (Figs 7b, 10e, 13a). Elongate scalenohedral or rhombohedral calcites surround clasts ranging from single quartz sand grains to large clasts of Devonian wall rock (Figs 10e, 13b). The paucity of contact points between the clasts suggests that the clasts are free to move away from one another. Fractured cockades (e.g. Fig. 13b) are locally preserved but the more widespread development of uniform overgrowths within and between clasts requires that the mineral cements grew evenly on all sides of each clast at the same rate. Whilst some of the concentric overgrowths may be the result of a "cut-effect" during sampling, the prevalence across multiple samples and paucity of contact points between clasts shows that the majority are "true" cockades. This suggests that they grew in either in suspension, and/or by repeated accretion and rotation

of clasts in an upwardly flowing, supersaturated fluid (Figs 13a, b; Frenzel & Woodcock 2014; Cox & Munroe 2016). More generally, the preservation of such textures indicates that the fracture cavities remained open for significant periods and were subject to episodic fluid fluxes with significant flow velocities. The open nature of the fissures is consistent with the filling with red sediment derived from above, and the ubiquity of this relationship suggests that complete sealing of mineralized fissures rarely occurred (see discussion in Frenzel & Woodcock 2014).

Crack-seal textures and fibrous calcite fills are preserved widely in dilational calcite veins in the Devonian basement rocks, where they also have a distinctly yellow colouration compared to the younger milky-white fissure fill calcites. These older features are widely interpreted to indicate the cyclic build-up of fluid pressures leading to repeated episodes of hydraulic fracturing and mineral precipitation (e.g. Ramsay 1980; Cox & Etheridge 1989). The absence of such features in the later mineralized Mode I fractures of inferred Permian age is consistent with the fissures remaining open or partially open due to their near surface location meaning that significant build-ups of fluid pressure that might lead to hydraulic fracturing (i.e. fault valve behaviour; Sibson 1990; Cox & Munroe 2016) did not occur.

Red sediment filling mechanisms

Sediment-filled fractures are commonly referred to in the literature as either “neptunian dykes” or “injectites” (Richter 1966; Martill & Hudson 1989; Siddoway & Gehrels 2014; Siddoway *et al.* 2019). Sediment that has been driven into a fracture cutting a low-permeability host rock in the sub-surface is commonly referred to as an “injectite” (Hurst *et al. 2011* and references therein). Injectites are generated where overpressure develops in a poorly consolidated, uncemented sandstone, leading to hydraulic fracturing in an adjacent (usually) overlying lithology, but they have also been recognised in crystalline basement

lithologies beneath unconformities (Siddoway & Gehrels 2014; Siddoway *et al.* 2019; Holdsworth et al. 2019). A lack of internal sedimentary structures is a characteristic feature of injectite sediment slurries (Walton & O'Sullivan 1950; Peterson 1967; Walker *et al.* 2013).

There is very little evidence for injection of sediment in the Tor Bay area. Whilst it is not ubiquitous, horizontal-bedding is locally observed within many cavity fills (Figs 3e, 4c, 5e, 6f, 8h, 13b), and the large euhedral, scalenohedral form of the calcite crystals that line the fracture cavities demonstrate that the voids were open prior to sediment infilling (Figs. 5e, 8c-h, 9e). Laminated sediment fills are also associated with a variety of geopetal structures which consistently young upwards and show that sediment progressively filled pre-existing open voids (Figs. 3e, 4c, 5e, 6f, 8c-h, 13b). The frequent lack of bedding laminations in many Tor Bay examples may be due to the periodic and repeated upward percolation of fluids through the sediment-filled fracture systems during and immediately following deposition, but prior to lithification (Fig. 11). This fluid flux could have been sufficient to destroy any sedimentary structures and cause a large-scale sorting/local homogenisation effect by elutriating the sediments and removing fines. Close to some of the larger basin-bounding faults, there is evidence of multiple fault movements at the same time as hydrothermal mineralization and sediment deposition. It is certainly conceivable that the repeated opening and closing of fault and fracture cavities in cohesive limestone basement close to the surface would lead to local fluid pressure changes. Hence it may be that finer silty fractions were able to be forced into open fractures following elutriation (Figs 11a-c). The result is a mass of sediment that has pervasively invaded any available and connected void space in the limestones below the regional base Permian unconformity.

Given the evidence for fluid flux through the sediment-filled fractures, it seems likely that some sediment was ejected from the fracture system and effused at the surface; but

has since been removed due to the erosive nature of the base-Permian unconformity. This would likely appear in the rock record as sand volcanoes, similar to those seen within some horizontal fault cavities (e.g. Fig 8e). Sand volcanoes are well reported in the rock record (Gill & Kuenen 1957; Rowe 2013), but are more commonly associated with liquefaction processes during seismic shaking, rather than co-seismic fluid flux. Large magnitude earthquakes such as the Christchurch earthquake (2011), Niigata (1964), and New Madrid (1812) have been shown to produce sand volcanoes at the surface as a result of co-seismic liquefaction processes. However, despite the lack of onshore examples, large offshore sub-marine mud volcanoes such as the Bortoluzzi volcano, offshore Calabria, frequently sit above major active fault zones and are formed through very similar processes (Cuffaro *et al.* 2019).

What drove fluid flow?

Whilst it is clear that the limestone-hosted fractures formed close to the surface and were open for long time periods, there is also evidence for cyclical, upward fluid fluxing events. Given the tectonic origin of the fissure systems and the clear association with active Permian rifting, it is likely that the migration of these fluids could be driven by co-seismic slip along larger basin bounding faults at depth (Sibson *et al.* 1975; Sibson 1981, 1994; Muir-Wood & King 1993). Semi-regular slip events along large faults will lead to changes in fault-void shape and volume, driving fluids out and drawing fluids in throughout the connected void network; suspending or rolling clasts around and precipitating minerals (Figs 13c, 14). Since the architecture of the observed fault voids are frequently irregular, curvilinear, and bifurcated, the opportunity to develop dilational jogs and props is widespread. As the faults accumulate slip, these jogs will open and close, creating and reducing fracture volumes and causing pressure changes, leading to the mobilisation of fluids and suspended sediment

throughout the connect cavity network. It is unknown whether the fluids involved here were meteoric or hydrothermal – or a mixture of both – and fluid inclusion and stable isotope analyses are required in order to ascertain the origins of the host fluids. Either way, a tectonic mechanism related to seismogenesis during rifting seems a plausible driving mechanism.

Implications for long-term fluid transport and storage

Since the marginal parts of many rift basins overlie regional erosional unconformities, there is every reason to extrapolate that similar sediment and mineral-filled fissure systems may form anywhere where the basement is strong and cohesive, e.g. massive carbonates, crystalline basement, and basalts. Examples of such fills from the geological record have been described in all these rock types (e.g. Angelier & Mechler 1977; Schlische & Ackermann 1995; Beacom *et al.* 1999; Walker *et al.* 2011; Siddoway & Gehrels 2014; Siddoway *et al.* 2019). Good modern examples are seen associated with the Dabbahu Fissure (Affar rift, in Ethiopia) (Rowland *et al.* 2007) and the mid-Atlantic ridge (Iceland) (Kettermann *et al.* 2019). These modern examples also feature fissures filled with surface detritus (sediment/lava/scree), and are formed along tectonic boundaries (Rowland *et al.* 2007; Kettermann *et al.* 2016, 2019). Similar structures to those studied here, such as zoned calcite mineralisation, are also reported in modern fissure systems (De Filippis *et al.* 2012).

As the basement subsides and is buried, the sediment and mineral fills prop open the highly interconnected network of cavities potentially maintaining the large apertures and connection pathways (Holdsworth *et al.* 2019, 2020). If the sediment within the cavities is largely free of clay due to the effects of elutriation, and is well sorted and distributed throughout the fracture network, it has the potential to preserve a high porosity and permeability, provided the pore space does not become completely occluded by mineral

cement. Whilst a detailed porosity analysis of the Tor Bay fissures has not been carried out in the present study, optical estimates from thin sections suggest local porosities of 10-35% which is significantly higher than in the surrounding Devonian limestones. This illustrates that these fracture fills are potentially important sites for the sub-surface storage of fluids in hydrocarbon basins, geothermal reservoirs, or aquifers.

The drone-based orthorectified virtual outcrop model (VOM) (Fig. 6a) and fracture trace map (Fig. 6b) from Shoalstone Beach illustrate in plan-view the very high interconnectivity of the sediment- and mineral-filled basement fissure systems formed in near surface settings (Figs 6a-d, g, h). A fracture topology plot (Fig. 6c; Sanderson & Nixon 2015) shows the connectivity of both the unfilled and sediment-filled fracture networks at Shoalstone Beach, with > 1.8 connections per fracture branch (> 1 is the threshold for a connected network). All sampled fracture networks show a dominance of Y-nodes over X- or I-nodes, though the unfilled network has more I-nodes, despite the higher number of fractures present. An areal calculation revealed that in fracture corridors like this, the percentage area of potentially highly permeable sandstone fill locally reaches up to 69%. Further details of the virtual outcrop modelling and analysis, including an attempt to estimate the total volumes of fracture fill can be found in Appendix A.

In the light of these findings, it is significant to note that the basal Permian-Triassic unconformities in the southern part of the UK are widely known to be associated with clastic and mineral infills (e.g. Woodcock et al. 2014, see their figure 13). For example, in Pembrokeshire, Carboniferous limestones are cut by large sediment- and mineral-filled faults and fractures, formed during the opening of the Bristol Channel Basin. The late-Triassic sediment fills here feature cockade textures, and geopetal accumulations, whilst the limestones show only minor karstic dissolution, and extensive brecciation (Wright *et al.*

2009; Woodcock *et al.* 2014). Arrays of red Triassic to early Jurassic sediment-filled fractures and faults also cut Carboniferous limestones in the Mendips (Williams 1986; Wall & Jenkyns 2004).

Collectively, our observations may explain why the basal Permo-Trias unconformity and underlying fractured basement are thought to form a significant aquifer and potential geothermal reservoir in the Southern British Isles. The unconformity is thought to provide an ingress point for fluids to generate substantial recent karst networks, potentially enabling deep-heat geothermal prospects (Narayan *et al.* 2018; and references therein). Faults and fractures with porous fissure fills will likely enhance the penetration of karstifying fluids, augmenting the potential for basement Devonian/Carboniferous limestones to be a significant geothermal reservoir. Fracture attribute and connectivity information collected in field sites such as the Shoalstone Beach outcrop could be important in helping to build better predictive fractured reservoir models.

Reactivation and timing relative to other regional events

Aside from the larger basin-bounding fault zones like those of Crystal Cove and Saltern Cove, there is relatively little evidence for reactivation of the fractures and associated fissure fills. An exception occurs at Hope's Nose. Mineralised fault breccias here are developed in Middle Devonian limestones (Russell 1929; Scrivener *et al.* 1994). These fault breccias trend broadly E-W (090-123^{o}) cross-cutting a set of unfilled N-S fractures. The presence of re-brecciated calcite breccia here (Fig. 7b) shows that the E-W faults and fracture corridors have been reactivated. Dendritic native gold, palladium, and haematite mineralization within the re-brecciated fractures was associated with localised acidic fluid alteration of calcite (Russell 1929; Scrivener *et al.* 1994). This chemically diverse, cross-course mineralisation has been dated at 236Ma ± 3Ma (mid to late Triassic) using Rb-Sr dating of

quartz by Scrivener *et al.* (1994). These authors suggested that the fluids were basinal brines originating from the Permo-Triassic New Red Sandstone and Aylesbeare mudstones. It is also plausible that they are a distal manifestation of the rifting responsible for the formation of fissures in the region of the Bristol Channel Basin to the northwest (Woodcock et al. 2014 and references therein). Collectively these observations illustrate that the initiation of the Portland-Wight Basin (Permian) was significantly earlier than the onset of rifting to form the Bristol Channel Basin (Triassic-Jurassic) in SW Britain.

Conclusions

The geological material found within fracture-hosted cavities hosted in basement rocks below regional unconformities preserves a valuable and under-utilised source of information regarding early basin histories. The fissure fill systems formed in the fractured Devonian limestones of the Tor Bay area (Fig. 14) are thought to have formed during early Permian NNW-SSE rifting, linked to early stages in the opening of the offshore Portland-Wight Basin. Cyclical and iterative precipitation of mainly calcite from circulating, possibly upwelling fluids occurred close to the surface (<1 km depth) in the fissures, plausibly related to repeated seismogenic faulting during rifting. At the same time, clastic sediments and wall rock fragments fell into, or were washed into, the open fault-related fissures from above (Figs 11, 14). Once incorporated, the sedimentary material in the fissures was commonly repeatedly remobilised, sorted, and redistributed by further episodes of fluid circulation throughout the near-surface fissure network. These fractures were very effectively propped open by their sediment and mineral fills and also by the inherent irregularity of the cavity walls, preserving their interconnectivity and potential permeability (Fig. 14). This may explain why the basal Permian-Triassic unconformities of southern Britain – which are

known to be widely associated with filled fissures of this kind - are associated with the development of significant regional geothermal reservoirs and aquifers. This is also likely to be the case globally in sub-unconformity settings of this kind.

Acknowledgments

This work was undertaken by Kit Hardman, as part of an on-going PhD studentship. The research in this paper was in part funded by the Institut Francias de Petrol Grant from the AAPG Grants-in-aid foundation – many thanks are given for their support. The authors also thank the structural research group members at Durham University for many helpful discussions, most notably Tom Utley and Zach Killingback, and the authors ever-patient partners. Reviewers Cathy Hollis, Nigel Woodcock and Editor Linda Kirstein all made very constructive and helpful suggestions to help improve the paper which are much appreciated.

References

Angelier, J. 1991. Inversion directe et recherche 4-D: comparaison physique et mathematique de deux modes de determination des tenseurs des paleocontraintes en tectonique de failles. *Comptes Rendus - Academie des Sciences, Serie II*, **312**, 1213–1218.

Angelier, J. & Mechler, P. 1977. Sur une methode graphique de recherche des contraintes principales egalement utilisables en tectonique et en seismologie : la methode des diedres droits. *Bulletin de la Societe Geologique de France*, **S7**-**XIX**, 1309–1318, https://doi.org/10.2113/gssgfbull.S7-XIX.6.1309.

Arthus-Bertrand, J. 2004. *Earth From Above*. Arthus-Bertrand, Jann.

Arthus-Bertrand, Y. 2020. Yann Arthus-Bertrand | Yann Arthus-Bertrand Photoshttp://www.yannarthusbertrand2.org/.

Beacom, L.E., Anderson, T.B. & Holdsworth, R.E. 1999. Using basement-hosted clastic dykes as syn-rifting palaeostress indicators: an example from the basal Stoer Group, northwest Scotland. *Geological Magazine*, **136**, 301–310, https://doi.org/10.1017/s0016756899002605.

Bott, M.H.P. 1959. The Mechanics of Oblique Slip Faulting. *Geological Magazine*, **XCVI**, 109–117, https://doi.org/10.1017/S0016756800059987.

Coward, M.P. & McClay, K.R. 1983. Thrust tectonics of S Devon. *Journal of the Geological Society*, **140**, 215–228, https://doi.org/10.1144/gsjgs.140.2.0215.

Cox, S.F. & Etheridge, M.A. 1989. *Coupled Grain-Scale Dilatancy and Mass Transfer during Deformation at High Fluid Pressures: Examples from Mount Lyell, Tasmania*.

Cox, S.F. & Munroe, S.M. 2016. Breccia formation by particle fluidization in fault zones: Implications for transitory, rupture-controlled fluid flow regimes in hydrothermal systems. *American Journal of Science*, **316**, 241–278, https://doi.org/10.2475/03.2016.02.

Cuffaro, M., Billi, A., et al. 2019. The Bortoluzzi Mud Volcano (Ionian Sea, Italy) and its potential for tracking the seismic cycle of active faults. *Solid Earth*, **10**, 741–763, https://doi.org/10.5194/se-10-741-2019.

De Filippis, L., Soligo, M., et al. 2012. Growth of fissure ridge travertines from geothermal springs of Denizli Basin, western Turkey. *Geological Society of America Bulletin*, **124**, 1629–1645, https://doi.org/10.1130/B30606.1.

Delvaux, D. & Sperner, B. 2003. *New Aspects of Tectonic Stress Inversion with Reference to the TENSOR Program*.

Delvaux, D., Moeys, R., Stapel, G., Melnikov, A. & Ermikov, V. 1995. Palaeostress reconstructions and geodynamics of the Baikal region, Central Asia, Part I. Palaeozoic and Mesozoic pre-rift evolution. *Tectonophysics*, **252**, 61–101, https://doi.org/10.1016/0040-1951(95)00090-9.

Dubois, C., Quinif, Y., et al. 2014. The process of ghost-rock karstification and its role in the

formation of cave systems. *Earth Science Reviews*, **131**, 116–148, https://doi.org/10.1016/j.earscirev.2014.01.006.
Ferrill, D.A. & Morris, A.P. 2003. Dilational normal faults. *Journal of Structural Geology*, **25**, 183–196, https://doi.org/10.1016/S0191-8141(02)00196-7.
Frenzel, M. & Woodcock, N.H. 2014. Cockade breccia: Product of mineralisation along dilational faults. *Journal of Structural Geology*, **68**, 194–206, https://doi.org/10.1016/j.jsg.2014.09.001.
García Carmona, J., Gómez Morales, J. & Rodríguez Clemente, R. 2003. Rhombohedral-scalenohedral calcite transition produced by adjusting the solution electrical conductivity in the system Ca(OH)2-CO2-H2O. *Journal of Colloid and Interface Science*, **261**, 434–440, https://doi.org/10.1016/S0021-9797(03)00149-8.
George Anniss, L. & Smith, S. 1927. The Geology of the Saltern Cove Area, Torbay. *Quarterly Journal of the Geological Society*, **83**, 492–500.
Gill, W. & Kuenen, P. 1957. Sand volcanoes on slumps in the carboniferous of County Clare, Ireland. *Quarterly Journal of the Geological Society*, **CXIII**, 441–460.
Guoyi Dong, Morrison, G. & Jaireth, S. 1995. Quartz textures in epithermal veins, Queensland - classification, origin, and implication. *Economic Geology*, **90**, 1841–1856, https://doi.org/10.2113/gsecongeo.90.6.1841.
Harvey, M.J., Stewart, S.A., Wilkinson, J.J., Ruffell, A.H. & Shail, R.K. 1994. Tectonic evolution of the Plymouth Bay Basin. *Geoscience in South-West England*, **8**, 271–278.
Hauselmann, P., Jeannin, P.-Y. & Bitterli, T. 1999. Relationships between karst and tectonics: case-study of the cave system north of Lake Thun (Bern, Switzerland). *Geodinamica Acta*, **12**, 377–388.
Healy, D., Rizzo, R.E., et al. 2017. FracPaQ: A MATLAB™ toolbox for the quantification of fracture patterns, https://doi.org/10.1016/j.jsg.2016.12.003.
Henson, M.R. 1971. *The Permo-Triassic Rocks of South Devon*. University of Exeter.
Holdsworth, R.E., McCaffrey, K.J.W., et al. 2019a. Natural fracture propping and earthquake-induced oil migration in fractured basement reservoirs. *Geology*, **47**, 700–704.
Holdsworth, R.E., Trice, R., et al. 2019b. The nature and age of basement host rocks and fissure fills in the Lancaster field fractured reservoir, West of Shetland. *Journal of the Geological Society*, https://doi.org/10.6084/m9.
Holloway, S. & Chadwick, R.A. 1986. The Sticklepath-Lustleigh fault zone: Tertiary sinistral reactivation of a Variscan dextral strike-slip fault. *Journal of the Geological Society*, **143**, 447–452, https://doi.org/10.1144/gsjgs.143.3.0447.
Hurst, A., Scott, A. & Vigorito, M. 2011. Physical characteristics of sand injectites. *Earth-Science Reviews*, **106**, 215–246, https://doi.org/10.1016/j.earscirev.2011.02.004.
Kettermann, M., Von Hagke, C., Van Gent, H.W., Grützner, C. & Urai, J.L. 2016. Dilatant normal faulting in jointed cohesive rocks: A physical model study. *Solid Earth*, **7**, 843–856, https://doi.org/10.5194/se-7-843-2016.
Kettermann, M., Weismuller, C., voc Hagke, C., Reicherter, K. & Urai, J.L. 2019. Large near-surface block rotations at normal faults of the Iceland rift: Evolution of tectonic caves and dilatancy. *Geology*.
Leveridge, B.E. & Hartley, A.J. 2003. The Variscan Orogeny : Devonian / Carboniferous basins in SW England and South Wales. 225–255.
Lundberg, J. & McFarlane, D. 2007. Pleistocene depositional history in a periglacial terrane: A 500 k.y. record from Kents Cavern, Devon, United Kingdom. *Geosphere*, **3**, 199–219, https://doi.org/10.1130/GES00085.1.
Martill, D.M. & Hudson, J.D. 1989. Injection clastic dykes in the Lower Oxford Clay (Jurassic) of central England: relationship to compaction and concretion formation. *Sedimentology*, **36**, 1127–1133, https://doi.org/10.1111/j.1365-3091.1989.tb01546.x.
Milodowski, A.E., Bath, A. & Norris, S. 2018. Palaeohydrogeology using geochemical, isotopic and mineralogical analyses: Salinity and redox evolution in a deep groundwater system through

Quaternary glacial cycles. *Applied Geochemistry*, **97**, 40–60, https://doi.org/10.1016/j.apgeochem.2018.07.008.
Muir-Wood, R. & King, G.C.P. 1993. Hydrological signatures of earthquake strain. *Journal of Geophysical Research: Solid Earth*, **98**, 22035–22068, https://doi.org/10.1029/93JB02219.
Narayan, N., Gluyas, J. & Adams, C. 2018. Is the UK in Hot Water. *Geoscientist*, **28**, 10–15, https://doi.org/10.1144/geosci2018-014.
Ortega, O.J., Marrett, R.A. & Laubach, S.E. 2006. A scale-independent approach to fracture intensity and average spacing measurement. *American Association of Petroleum Geologists Bulletin*, **90**, 193–208, https://doi.org/10.1306/08250505059.
Paquette, J., Ward, W.B. & Reeder, R.J. 1993. Compositional Zoning and Crystal Growth Mechanisms in Carbonates: A New Look at Microfabrics Imaged by Cathodoluminescence Microscopy. Springer, New York, NY, 243–252., https://doi.org/10.1007/978-1-4684-9421-1_18.
Peterson, G.L. 1967. Flow structures in sandstone dikes. *Sedimentary Geology*, **2**, 177–190, https://doi.org/10.1016/0037-0738(68)90024-9.
Petit, J.P. 1987. Criteria for the sense of movement on fault surfaces in brittle rocks. *Journal of Structural Geology*, **9**, 597–608, https://doi.org/10.1016/0191-8141(87)90145-3.
Popov, P., Qin, G., Bi, L., Efendiev, Y., Ewing, R. & Li, J. 2009. Multiphysics and multiscale methods for modeling fluid flow through naturally fractured carbonate karst reservoirs. *SPE Reservoir Evaluation & Engineering*, **12**, 218–231, https://doi.org/10.2118/105378-PA.
Ramsay, J.G. 1980. The crack-seal mechanism of rock deformation. *Nature*, **284**, 135–139.
Richter, D. 1966. On the New Red Sandstone Neptunian dykes of the Tor Bay area (Devonshire). *Proceedings of the Geologists' Association*, **77**, 173-IN3, https://doi.org/10.1016/S0016-7878(66)80068-8.
Rowe, C. 2013. Shaking Loose: Sand volcanoes and Jurassic earthquakes. *Geology*, **41**, 1135–1136.
Rowland, J., Baker, E., et al. 2007. Fault growth at a nascent slow-spreading ridge: 2005 Dabbahu rifting episode, Afar. *Geophysics Journal International*, **171**, 1226–1246.
Ruffell, A.H. & Shelton, R.G. 2000. Permian to Late Triassic post-orogenic collapse and early Atlantic rifting, deserts, evaporating seas and mass extinctions. *In*: Woodcock, N. & Strachan, R. (eds) *Geological History of Britain and Ireland*. Oxford, Blackwell Science Ltd, 297–313.
Russell, A. 1929. On the occurrence of native gold at Hope's Nose, Torquay, Devonshire.
Sanderson, D.J. & Nixon, C.W. 2015. The use of topology in fracture network characterization. *Journal of Structural Geology*, **72**, 55–66, https://doi.org/10.1016/j.jsg.2015.01.005.
Schlische, R.W. & Ackermann, R. V. 1995. Kinematic significance of sediment-filled fissures in the North Mountain Basalt, Fundy rift basin, Nova Scotia, Canada. *Journal of Structural Geology*, https://doi.org/10.1016/0191-8141(94)00114-F.
Scrivener, R.C., Darbyshire, D.P.F. & Shepherd, T.J. 1994. Timing and significance of crosscourse mineralization in SW England. *Journal of the Geological Society*, **151**, 587–590, https://doi.org/10.1144/gsjgs.151.4.0587.
Shail, R.K. & Leveridge, B.E. 2009. The Rhenohercynian passive margin of SW England: Development, inversion and extensional reactivation. *Comptes Rendus - Geoscience*, **341**, 140–155, https://doi.org/10.1016/j.crte.2008.11.002.
Shail, R.K. & Wilkinson, J.J. 1994. Late- to post-Variscan extensional tectonics in south Cornwall. *Proceeding of the Ussher Society*, **8**, 262–270.
Shannon, W.G. 1928. The geology of the Torquay district. *Proceedings of the Geologists' Association*, **39**, 103-IN2, https://doi.org/10.1016/S0016-7878(28)80020-4.
Shepard, T.J., Bouch, J.E., et al. 2005. Permo-Triassic unconformity-related Au-Pd mineralisation, South Devon, UK: new insights and the European perspective. *Mineralium Deposita*, **40**, 24–44, https://doi.org/10.1007/s00126-004-0459-3.
Sibson, R.H. 1981. Fluid flow accompanying faulting: Field evidence and models. *Earthquake prediction*, **4**, 593–603, https://doi.org/10.1029/ME004p0593.
Sibson, R.H. 1990. Conditions for fault-valve behaviour. *In*: Knipe, R. J. & Rutter, E. H. (eds)

Deformation Mechanisms, Rheology and Tectonics. London, Geological Society Special Publication, 15–28.
Sibson, R.H. 1994. Crustal stress, faulting and fluid flow. *Geological Society, London, Special Publications*, **78**, 69–84, https://doi.org/10.1144/GSL.SP.1994.078.01.07.
Sibson, R.H. 1996. Structural permeability of fluid-driven fault-fracture meshes. *Journal of Structural Geology*, **18**, 1031–1042, https://doi.org/10.1016/0191-8141(96)00032-6.
Sibson, R.H., Moore, J.M.M. & Rankin, A.H. 1975. Seismic pumping - a hydrothermal fluid transport mechanism. *Journal of the Geological Society*, **131**, 653–659, https://doi.org/10.1144/gsjgs.131.6.0653.
Siddoway, C.S. & Gehrels, G.E. 2014. Basement-hosted sandstone injectites of Colorado: A vestige of the Neoproterozoic revealed through detrital zircon provenance analysis. *Lithosphere*, **6**, 403–408, https://doi.org/10.1130/L390.1.
Siddoway, C.S., Palladino, G., Prosser, G., Freedman, D. & Duckworth, & W.C. 2019. Basement-hosted sand injectites: use of field examples to advance understanding of hydrocarbon reservoirs in fractured crystalline basement rocks, https://doi.org/10.1144/SP493-2018-140.
Smart, P.L., Palmer, R.J., Whitaker, F. & Paul Wright, V. 1988. Neptunian Dikes and Fissure Fills. *In*: James, N. P. & Choquette, P. W. (eds) *Paleokarst*. New York, Springer, 149–150.
Smith, K.G. 1952. Structure plan of clastic dikes. *Eos, Transactions American Geophysical Union*, **33**, 889–892, https://doi.org/10.1029/TR033i006p00889.
Strange P. J. 2001. Torquay 1:50 000 Geology series map. *NERC, OS*, 1.
Thomas, H.H. 1909. A contribution to the petrography of the new red sandstone in the West of England. *Geological society of London*, **65**, 229–244.
Trice, R. 2005. Challenges and Insights in Optimizing Oil Production from Middle East Mega Karst Reservoirs.
Underhill, J.R. & Stoneley, R. 1998. Introduction to the development, evolution and petroleum geology of the Wessex Basin. *Geological Society, London, Special Publications*, **133**, 1–18, https://doi.org/10.1144/GSL.SP.1998.133.01.01.
Ussher, W.A.E. 1903. The geology of the country around Torquay : Explanation of sheet 350. *Memoirs of the Geological Survey of Great Britain, England and Wales (Sheet - New Series)*.
van Gent, H.W., Holland, M., Urai, J.L. & Loosveld, R. 2010. Evolution of fault zones in carbonates with mechanical stratigraphy - Insights from scale models using layered cohesive powder. *Journal of Structural Geology*, **32**, 1375–1391, https://doi.org/10.1016/j.jsg.2009.05.006.
von Hagke, C., Kettermann, M., Bitsch, N., Bücken, D., Weismüller, C. & Urai, J.L. 2019. The effect of obliquity of slip in normal faults on distribution of open fractures. *Frontiers in Earth Science*, **7**, 18, https://doi.org/10.3389/feart.2019.00018.
Walker, R.J., Holdsworth, R.E., Imber, J. & Ellis, D. 2011. The development of cavities and clastic infills along fault-related fractures in Tertiary basalts on the NE Atlantic margin. *Journal of Structural Geology*, **33**, 92–106, https://doi.org/10.1016/j.jsg.2010.12.001.
Walker, R.J., Holdsworth, R.E., Imber, J., Faulkner, D.R. & Armitage, P.J. 2013. Fault zone architecture and fluid flow in interlayered basaltic volcaniclastic- crystalline sequences. *Journal of Structural Geology*, **51**, 92–104, https://doi.org/10.1016/j.jsg.2013.03.004.
Wall, G.R.T. & Jenkyns, H.C. 2004. The age, origin and tectonic significance of Mesozoic sediment-filled fissures in the Mendip Hills (SW England): implications for extension models and Jurassic sea-level curves. *Geological Magazine*, **141**, 471–504, https://doi.org/10.1017/S0016756804009185.
Wallace, R.E. 1951. Geometry of Shearing Stress and Relation to Faulting. *The Journal of Geology*, **59**, 118–130, https://doi.org/10.1086/625831.
Walton, M.S.J. & O'Sullivan, R.B. 1950. The intrusive mechanics of a clastic dike. *American Journal of Science*, **248**, 1–21.
Williams, G.D. 1986. The Bristol-Mendip foreland thrust belt. *Journal of the Geological Society*, **143**, 63–73, https://doi.org/10.1144/gsjgs.143.1.0063.

Woodcock, N.H., Miller, A.V.M. & Woodhouse, C.D. 2014. Chaotic breccia zones on the Pembroke Peninsula, south Wales: Evidence for collapse into voids along dilational faults. *Journal of Structural Geology*, **69**, 91e107, https://doi.org/10.1016/j.jsg.2014.09.019.

Wright, V., Woodcock, N.H. & Dickson, J.A.D. 2009. Fissure fills along faults: Variscan examples from Gower, South Wales. *Geological Magazine*, **146**, 890–902, https://doi.org/10.1017/S001675680999001X.

Yang, H., Zhu, G., Wang, Y., Su, J. & Zhang, B. 2014. *The Geological Characteristics of Reservoirs and Major Controlling Factors of Hydrocarbon Accumulation in the Ordovician of Tazhong Area, Tarim Basin*.

Figure captions

Fig. 1) (a) Hypothetical Mohr circles illustrating the translation from tensile failure at the surface to normal faulting (shear fracture) at depth (after van Gent et al. 2010). (b) Cross section view of fractures generated in analogue model (van Gent et al. 2010) illustrating fault cavity architectures for different depth zones. (c) Aerial photograph of Thingvellir Rift, Iceland howing large tensile fissures developed in basalts at the surface related to the development of a normal fault at depth. Photograph used with permission by Yann Arthus-Bertrand, part of the Earth from Above collection - www.yannarthusbertrand2.org (Arthus-Bertrand 2004, 2020).

Fig. 2) Left: Simplified location map of Tor Bay, with key locations and study areas shown by red boxes. Right: Simplified coastal onshore-offshore geological map of main lithological and stratigraphic units and structures in Tor Bay. Adapted from British Geological Survey 2004, Harvey et al. (1994), and data provided with permission by EDINA Digimap:

(OS VectorMap® Local [TIFF geospatial data], OS Terrain 5 [ASC & SHAPE geospatial data] Scale 1:10000, Tiles: sx85ne, sx85se, sx86ne, sx86se, sx95ne, sx95nw, sx95sw, sx96ne, sx96nw, sx96se, sx96sw, Updated: 27 June 2018, Ordnance Survey (GB), Using: EDINA Digimap Ordnance Survey Service, <https://digimap.edina.ac.uk>)

(DiGRock250k [SHAPE geospatial data], Scale 1:250000, Tiles: GB, Updated: 31 December 2013, BGS, Using: EDINA Geology Digimap Service, <https://digimap.edina.ac.uk>)

(DiGMapGB-50 [SHAPE geospatial data], Scale 1:50000, Tiles: ew339,ew350, Updated: 30 November 2016, BGS, Using: EDINA Geology Digimap Service, <https://digimap.edina.ac.uk>)

Fig. 3) Field photographs and location map of large faults at Crystal Cove (for location see Fig. 2). (a) Maps showing key location names (left) and basic geology (right). For key see Fig. 2. (b) View of large fault surface separating Devonian limestone (DL) and Torbay Breccia Formation (TBf) with a 'wall' of geopetal clastic sediment infill and calcite mineralisation (Ca). Locations of Figs 3c and e are also shown [SX89702 58039]. (c) Cross-section view of the large fault shown in (b), showing c. 40m wide "v" shaped fault aperture filled with red sandstone-breccia and complex calcite mineralisation [SX89541 57918]. (d) Slickenlines seen on fault wall at contact between fault sediment infill and limestone host rock along the major fault seen in (c) [SX89541 57918]. (e) Geopetal sediment accumulation in a conical shaped pile within a calcite mineralised fault plane, location given in (b) [SX89590 57996]. (f) Plan view of fault cavity infill with successive syntaxial calcite mineralisation and sediment infilling giving strata-like banded appearance reflective of repeated opening history [SX89619 58614]. (g) Stereographic projection of contoured poles to shear fracture planes, mean cyclographic shear plane, slickenline lineations, and tensile fracture planes.

Fig. 4) Virtual Outcrop Model and field photographs from Saltern Cove (for location see Fig . 2). (a) Annotated 3D virtual outcrop model. Inset shows the stereographic projection of data from the reverse/thrust fault and slickenlines, the dilatant fault, and the bedding of the overlying limestone and a bedding-parallel fold axis [SX89488 58535]. (b) Local geological map, with main outcrops labelled; for key see Fig 2. (c) Section view of bedded sediment

overlying the fallen limestone block. Location shown in (a). (d) Zoned volcaniclastic tephra within the tensile normal fault; orange material is fine grained tuff, with suspended volcanic clasts. (e) Breccia material infilling the normal tensile fault, with clasts of brecciated orange volcaniclastic material set in a red sandstone matrix. (f) Cross section view of limestone-hosted vuggy calcite-lined cavities in the hangingwall of the thrust fault.

Fig. 5) Field photographs, maps and structural data from Berry Head (for location see Fig. 2). (a) Digitised field sketch map showing locations and orientations of the sediment-filled fractures on headland (black lines), with inset (left) oblique view of Berry Head from Google Earth, with locations labelled. The yellow box is the location of Berry Head Quay. Second inset (right) shows a stereonet showing poles to fracture planes and mean cyclographic plane (red), demonstrating the general ENE-WSW strike and SE dip. Basemap 5m digital elevation model (scale shown) generated from Ordnance Survey data provided with permission by Edina Digimap (OS Terrain 5 [XYZ geospatial data], Scale 1:10000, Tiles: sx95nw, Updated: 3 December 2019, Ordnance Survey (GB), Using: EDINA Digimap Ordnance Survey Service, <https://digimap.edina.ac.uk>). (b) Plan view of jigsaw breccia in fracture cavity [SX94418 56714]. (c) View of quarry face showing red sandstone infilling and calcite vein development and cross-cutting relationships within vertical fracture cavities in limestone [SX94296 56619]. (d) Section view of sub-horizontal smaller fracture cavities and "linked-flats" infilled with red sandstone, W Berry Head Quarry [SX94156 56566]. (e) Bedded red sandstone within a small irregular shaped cavity bound by syntaxial sparry calcite growth [SX94418 56714]. (f) Large sandstone-filled sub-vertical dilatant cavity (right) and bifurcated smaller cavity (left) at Berry Head Quay [SX94418 56714].

Fig. 6) Orthorectified outcrop images and trace maps, data and field photographs from Shoalstone Beach (for location see Fig. 2). (a) Virtual Outcrop Model in which smallest structures resolvable are 1.5-2.5cm. (b) Interpreted fracture-trace map. Sediment-filled fractures in orange, unfilled fractures in black. (c) Sediment-filled fracture-volume map, interpreted from within well exposed selected area shown. Note the irregularity of apertures and traces. A summary fracture volume estimates is also given; for more information, see Appendix A. (d) Fracture topology plot of fracture node types showing connectivity (Sanderson & Nixon 2015). Manual and automated (Healy *et al.* 2017) analyses show that both the unfilled and filled fractures are well connected. (e) Rose diagrams of fracture segment strike angles generated using FracPaQ MATLAB toolbox, with average strike in red, showing that sediment-filled fractures are strongly orientated in ENE-WSW and N-S orientations. (f) Section view of well-bedded sandstone fracture fill and calcite veining from east of Shoalstone Beach [SX 93834 56770]. (g) View of single fracture c.4.5m in aperture, filled with a uniform, homogenous unbedded red sandstone [SX 93696 56789]. (h) Interconnected fracture network filled with homogenous red sandstone with no calcite veins lining the wall-rock contacts [SX 93775 56780].

Fig. 7) Field photographs and structural data from Hope's Nose. (a) Section view of red sandstone-filled, lozenge-shaped sub-vertical fracture cavities showing minor dissolution of the limestone host rock and early karstification prior to deposition of infill. Mdt = Devonian Meadfoot Group [SX 94932 63666]. (b) Multiphase mineralised breccia. Clasts include limestone, mudstone, and earlier brecciated calcite, cemented by secondary calcite and darker ore minerals (arrowed). (c) Section view of 'fracture stratigraphy' showing dilatant fracturing in thickly bedded limestones below, and shallower dipping narrow shear fracture

in thinly bedded mudstones above [SX 94942 63705]. (d) Section view of forced fold in finer bedded units. (e) Stereonet showing poles to fracture planes and slickenline lineations from Hope's Nose, with mean plane and vector data shown in red [SX 94952 63634].

Fig. 8) Field photographs of fissure fills from key outcrops around Fishcombe Point and Fishcombe Cove. (a) & (b) Local geological map, and stereonet showing poles to sediment-filled fracture planes for Elberry and Fishcombe, demonstrating E-W and N-S trends as seen in mean cyclographic planes (N-S in red, E-W in blue); the dark red dashed line corresponds to the large fault at Fishcombe Cove. For key to geological map see Fig. 2. (c) Section view of subvertical sediment-filled fault cavity at Fishcombe Point – white lines, and two sets of subhorizontal fault cavities intersecting – highlighted in yellow. Host rocks are folded Devonian limestones and interstitial mudstones of the Brixham Limestone Formation – BxL. Locations of (d)-(f) are also shown [SX 91825 57062]. (d) Section view of horizontal fracture cavities showing the relationships between calcite mineralisation, minor-limestone dissolution, and sediment infilling. (e) Sand-volcano structures at the intersection of vertical and horizontal fractures. Note the conical shape and central vent, and apparent fingering of sediment down-slope. (f) Section view of horizontal cavity partially filled with red siltstone-sandstone, with the tips of scalar scalenohedral calcite crystals poking through the top-surface. (g) Section view of large red sandstone-filled cavity with calcite lining at Fishcombe Cove. Location of (h) is shown by black box [SX 91979 56929]. (h) Close up of red sandstone-filled fracture cavity in (g), bound by thick calcite veins. Sediment is bedded showing geopetally inclined and horizontal beds in addition to a single well-developed flame structure, all highlighted in yellow. (i) View of cross cutting red sandstone-filled fractures at

Fishcombe Cove, younger N-S set picked out in white, older E-W set highlighted in yellow [SX 91976 56949].

Fig. 9) Field photographs of calcite mineralisation types found in fracture cavities around Tor Bay. (a) Simple scalenohedral (dog tooth spar) calcite, Crystal Cove [SX 89615 58018]. (b) Complex scalar scalenohedral calcites growing in a sub-horizontal fracture cavity, Fishcombe Point [SX 91828 57061]. (c) Rhombohedral (nail head spar) sparry calcite, Crystal Cove [SX 89615 58018]. (d) Euhedral cubic calcites, Crystal Cove [SX 89586 57977]. (e) Splaying "plumose" calcites later partially filled with sandstone in a loose boulder found near Broadsands Beach [SX 89615 58018]. (f) Colour zonations in individual calcite crystals showing variations in hematite content, Crystal Cove [SX 89586 57977]. (g) Travertine mineralisation, Hope's Nose quarry [SX 94924 63660].

Fig. 10) Thin section photomicrographs of sediment infills. (a) PPL image of sub-rounded red sandstone grains in contact with a calcite vein. Quartz sand grains are coated in a thin rim of haematite. The calcite vein grows in optical continuity with the sandstone cement. (b) Thin section chip from a fracture fill at Shoalstone Beach showing the multiphase calcite vein – sediment infilling relationships. (c) PPL image of red sandstone infilling gap between two scalenohedral calcite crystals. Note lack of compaction and high porosity (blue stain). (d) PPL image of heavily cemented red sandstone infilling fracture cavity, showing paucity of contact points between grains. (e) PPL image of fine-grained red silt from sub-horizontal cavity, consisting of material likely elutriated from nearby vertical sandstone-filled fracture. (f) PPL image of cockade-style quartz mineralisation of individual grains, with intergranular porosity (blue). Rounded quartz grains with a thin hematite coating, are enclosed by quartz

cement growing in optical continuity with the clastic grains. (g) XPL image of (f), highlighting the optical continuity of the cockade style quartz cement surrounding each quartz grain – separated by a thin haematite coating.

Fig. 11) Fissure fill elutriation and emplacement sorting processes. (a) Illustration of near-surface fault architectures and the sorting of unconsolidated infills by fluid flow. i) Emplacement sorting process where fine material is held in suspension by fluid and is unable to enter the fracture system, whilst coarser material rolling around on the palaeosurface is able to fall in. ii) Elutriation of finer sediment by fluid percolating vertically through the fracture-hosted unconsolidated sediment. Coarser material is held in or falls out of suspension, whereas fine material is winnowed out. This fine material is then either deposited where the fluid velocity drops in horizontal or dead-end fractures; or is expelled at the palaeosurface. (b) Section view of sub-vertical to sub-horizontal filled-fracture linkage, showing fining of fill in the horizontal fracture away from the vertical cavity. Taken at Fishcombe Cove [SX 92021 56996]. (c) Plan view of subvertical fracture in (b), showing cockade style calcite mineralisation around angular clasts of Devonian mudstone (Dm) and Brixham Limestone (BxL). Host rock is Brixham Limestone suggesting upward migration of older Devonian mudstone clasts in cavity. Note the near uniform clast size, and lack of fines despite the proximity to the fine red sedimentary material shown in (b).

Fig. 12) Palaeostress analysis of slip vectors (slickenlines) from major fault planes using WinTensor (Delveaux, 1995; Angelier, 1997). Results tabulated above and illustrated in stereonet projections below.

Fig. 13) Examples and models of multiphase breccia formation. (a) Fault breccia from Petit Tor Point displaying cockade style mineralisation, with clasts of angular limestone separated by calcite mineralisation. Varying from other cockade style fabrics in Tor Bay as the thickness of calcite veining varies [SX 92649 66144]. (b) Section view of fault infill from Crystal Cove, showing fractured cockade-style brecciation, mineralisation, and geopetal sediment infilling around clasts of suspended older wall rock [SX 89541 57918]. (c) Panelled illustration of formation of fault infill seen in (b), from repeated fault movement, fluid flux events and passive sedimentary infilling.

Fig. 14) Schematic synoptic illustration of a typical near surface, mineral- and sediment-filled fault and fissure system and processes hosted in carbonate basement based on observations in the Tor Bay area.

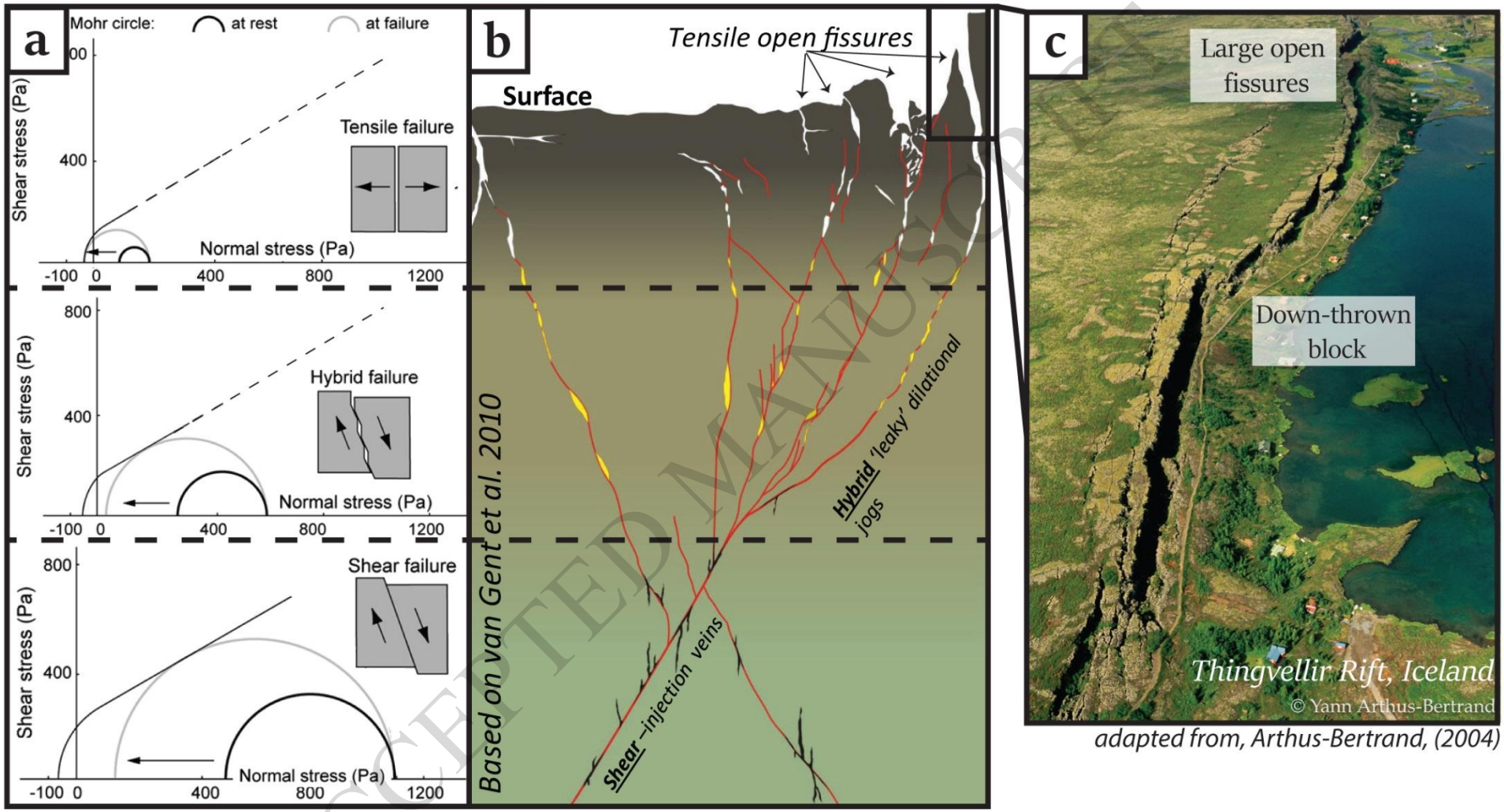

adapted from, Arthus-Bertrand, (2004)

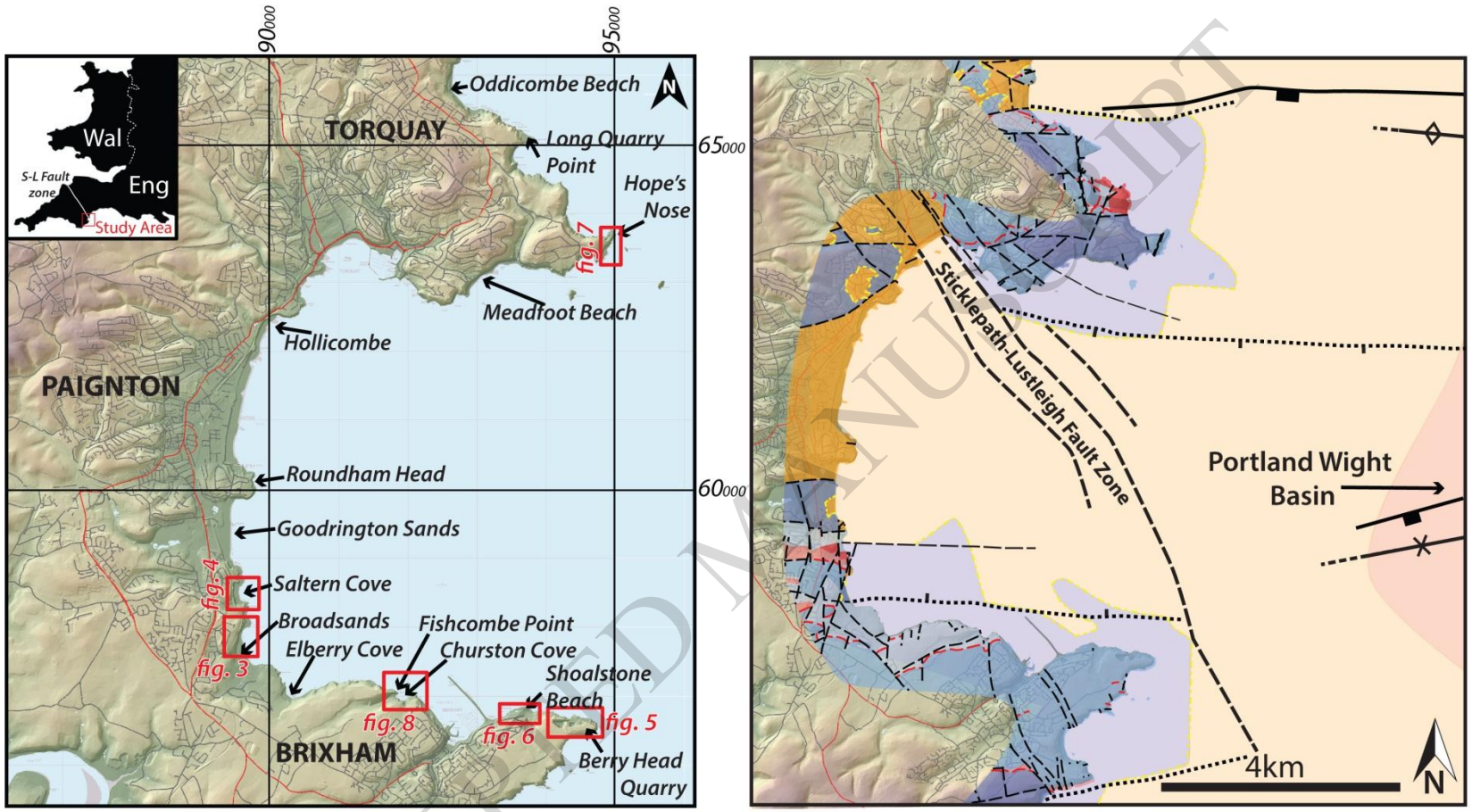

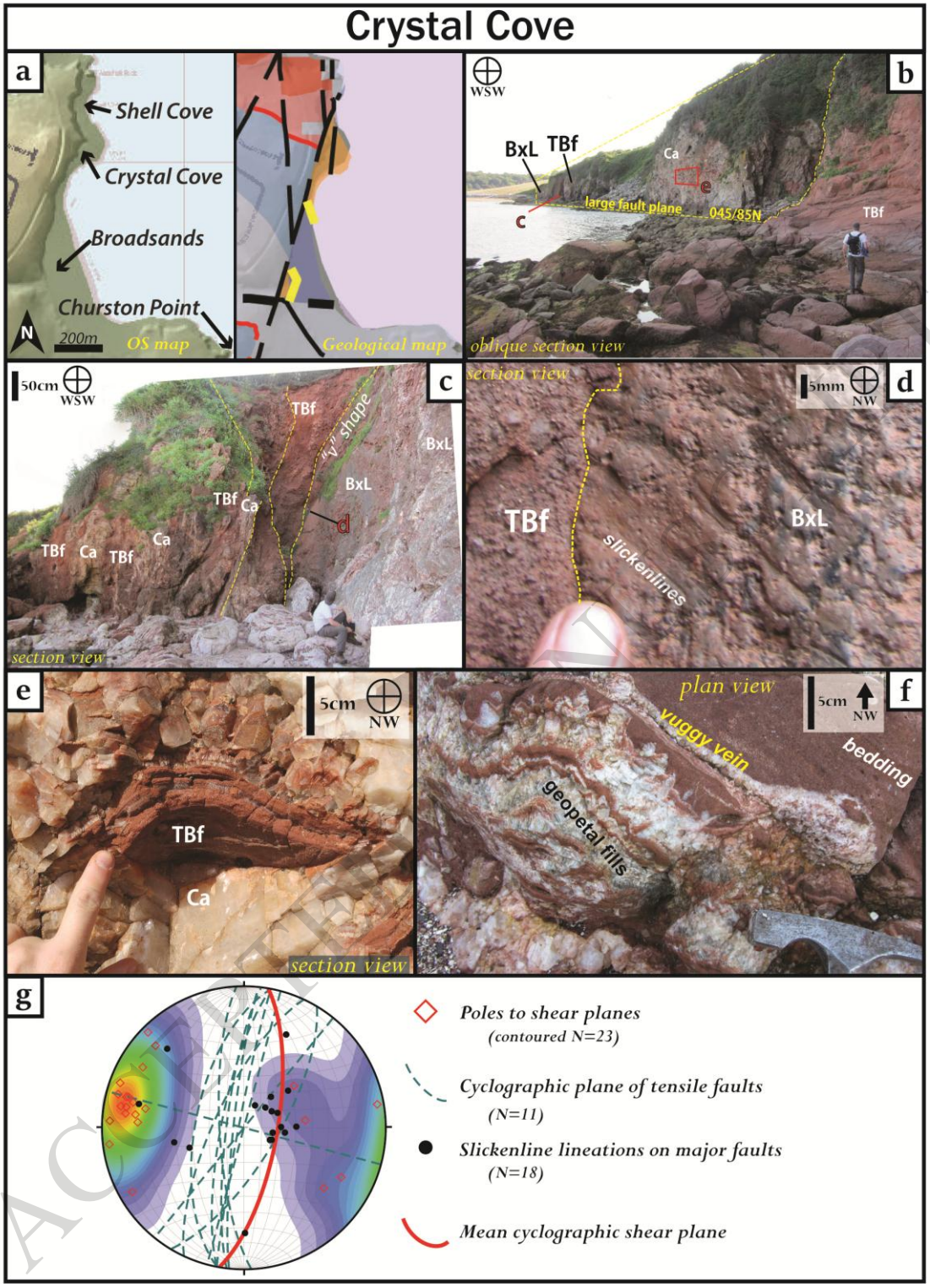

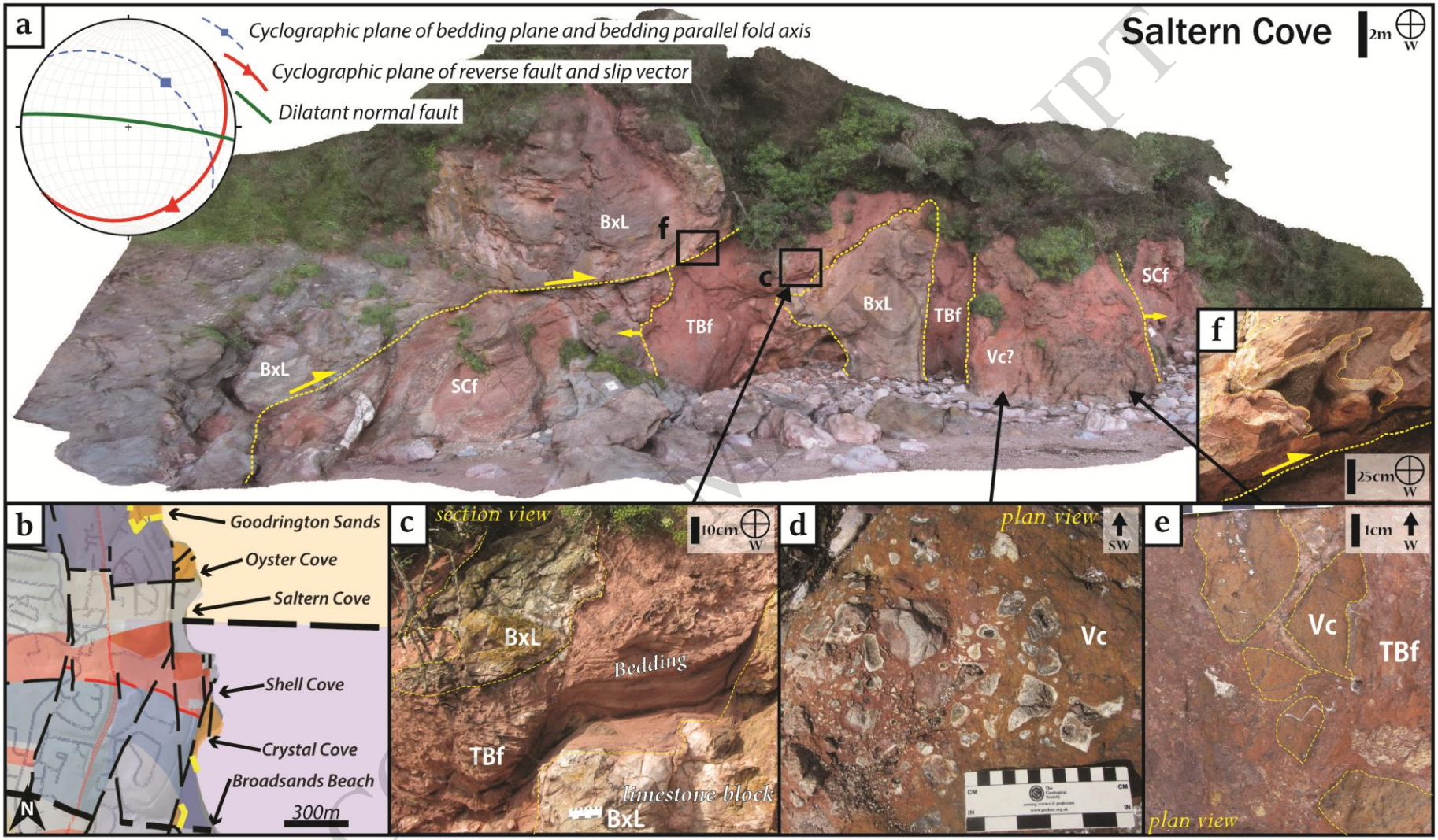

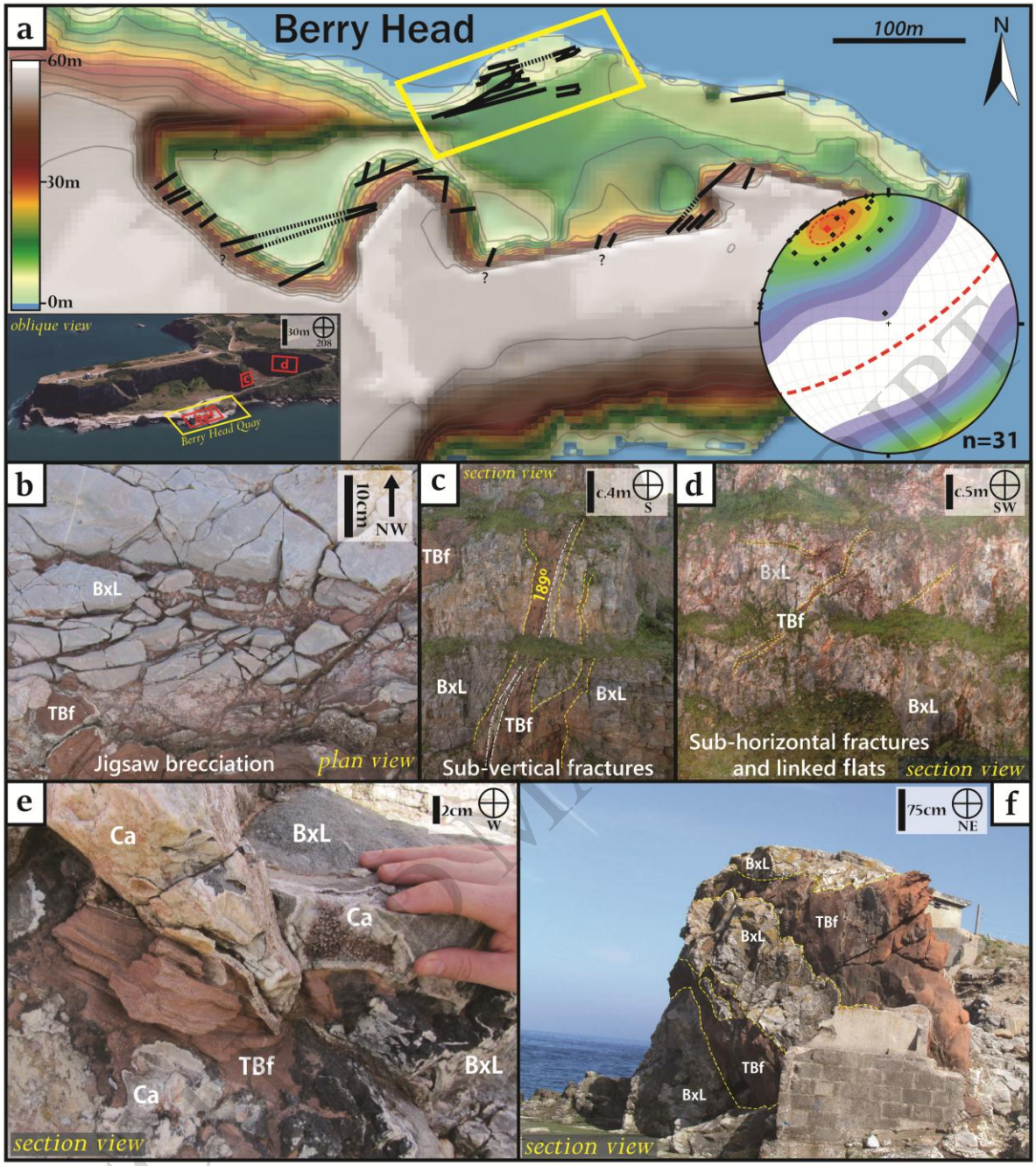

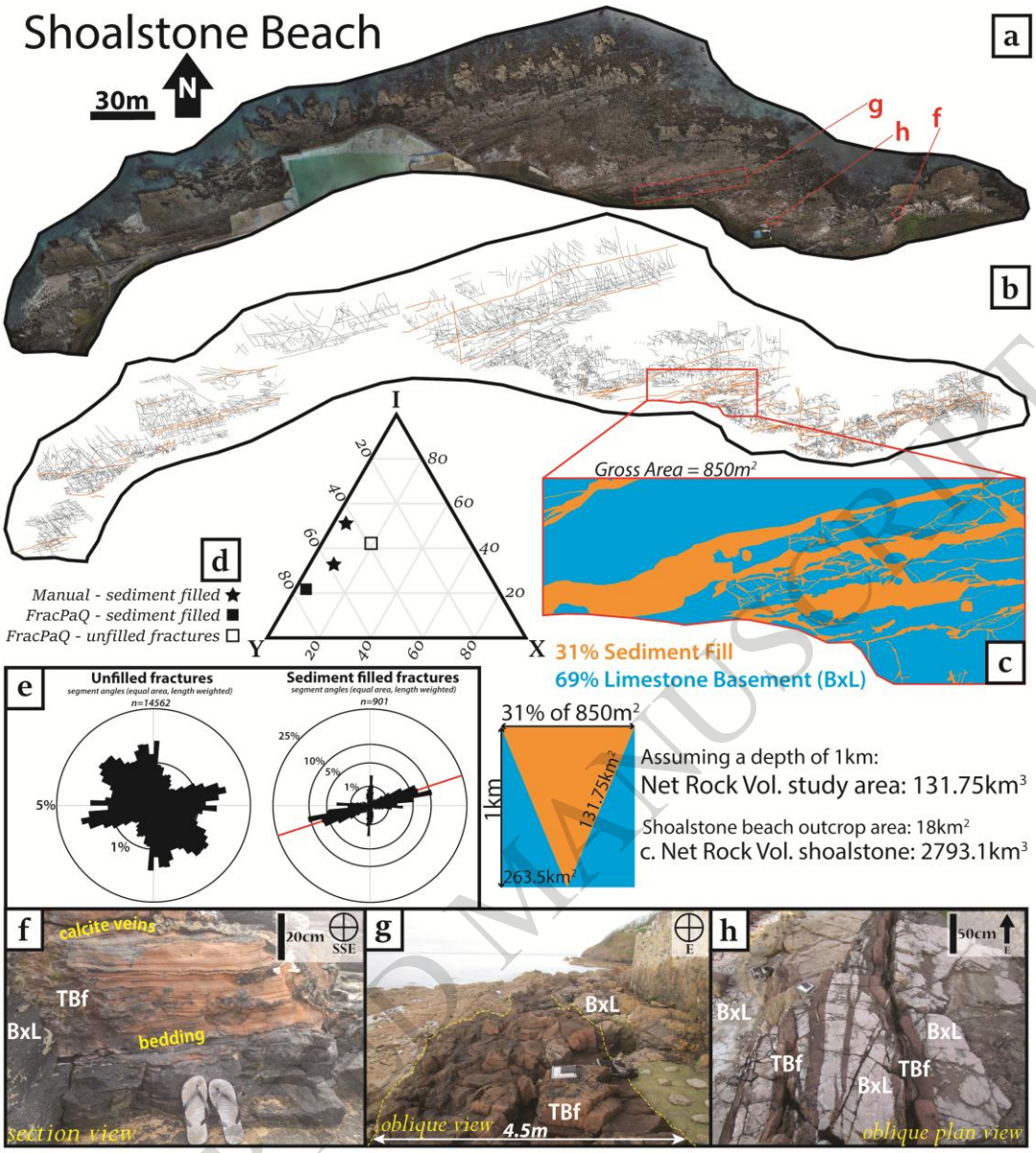

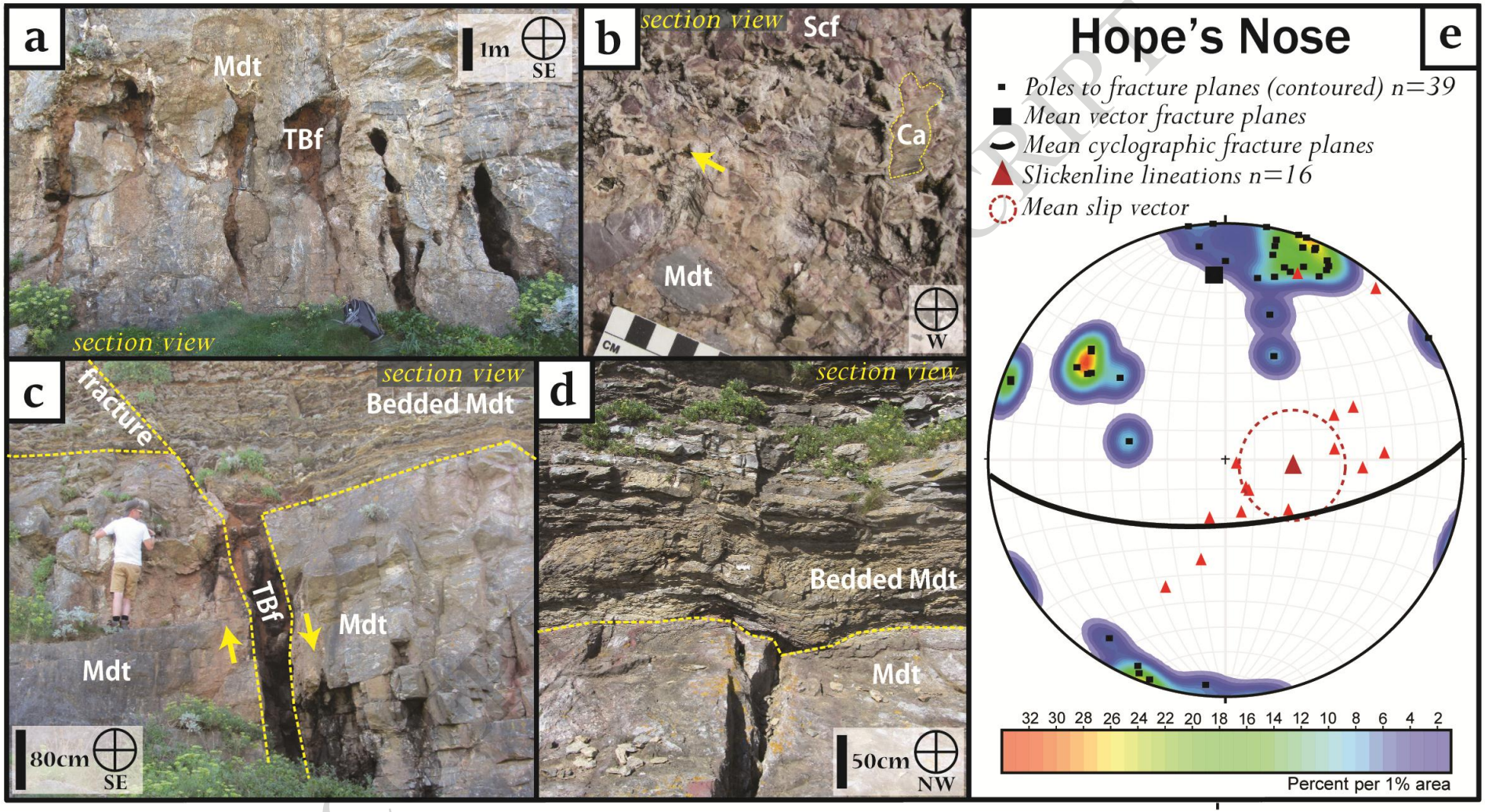

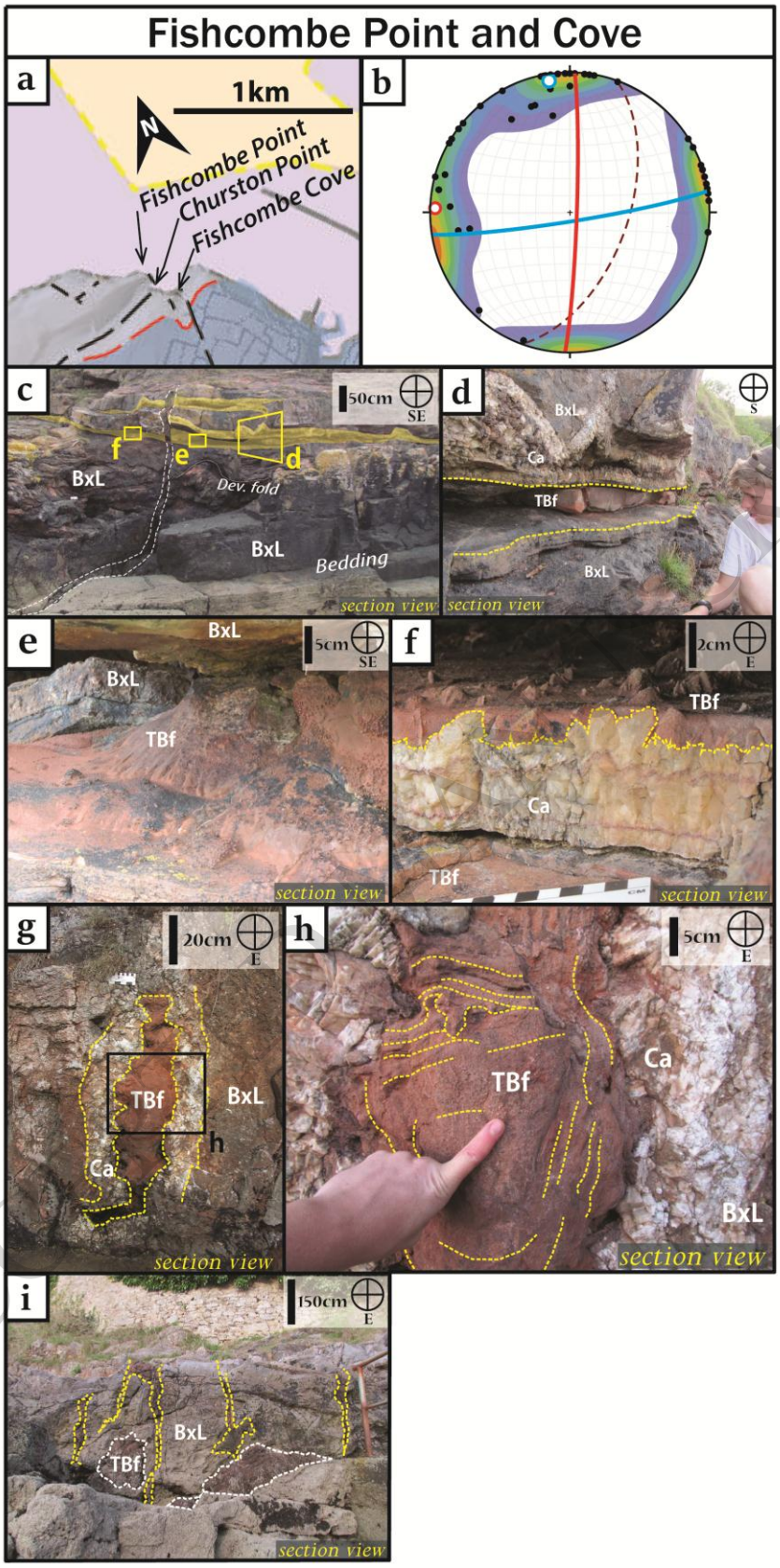

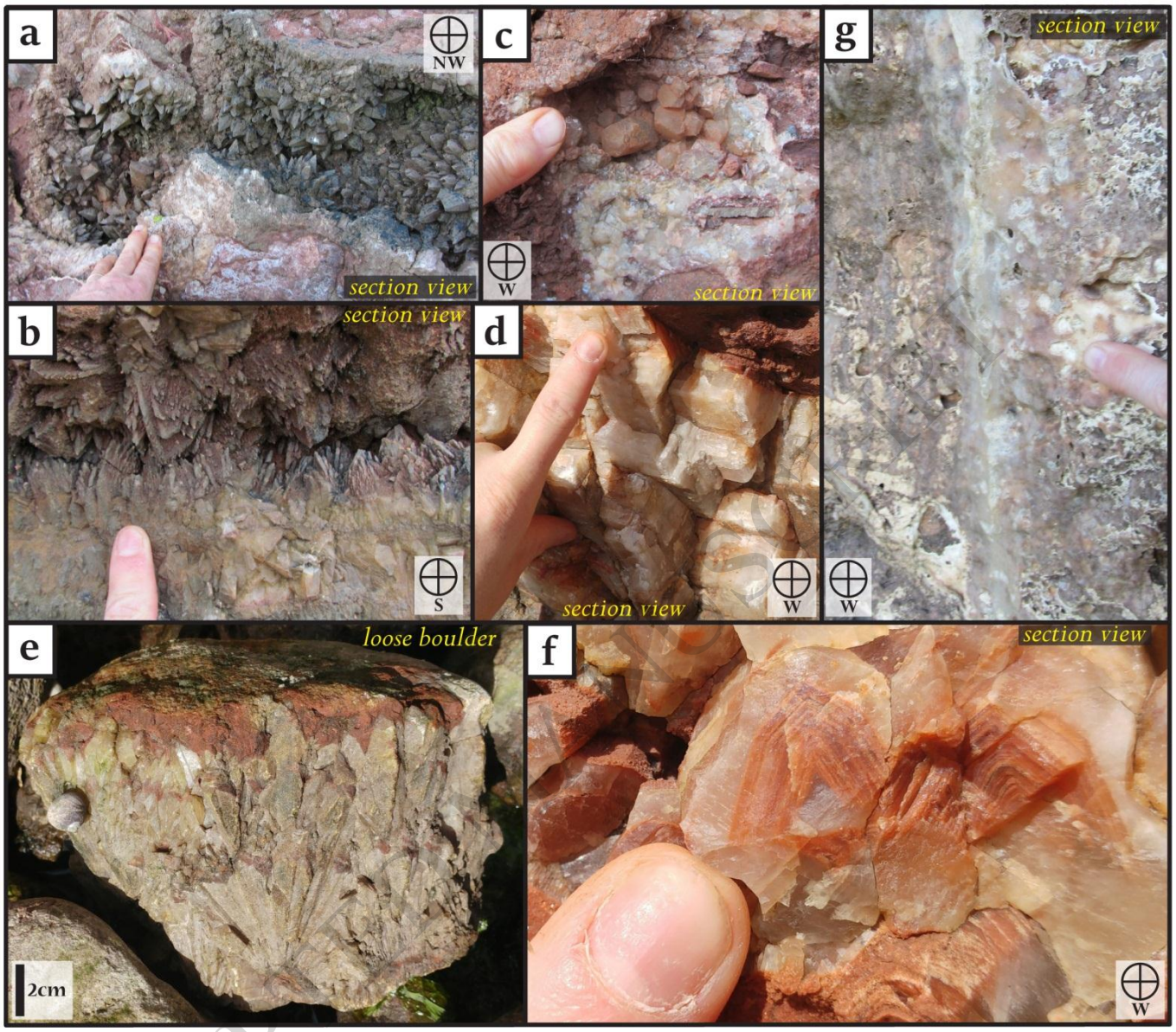

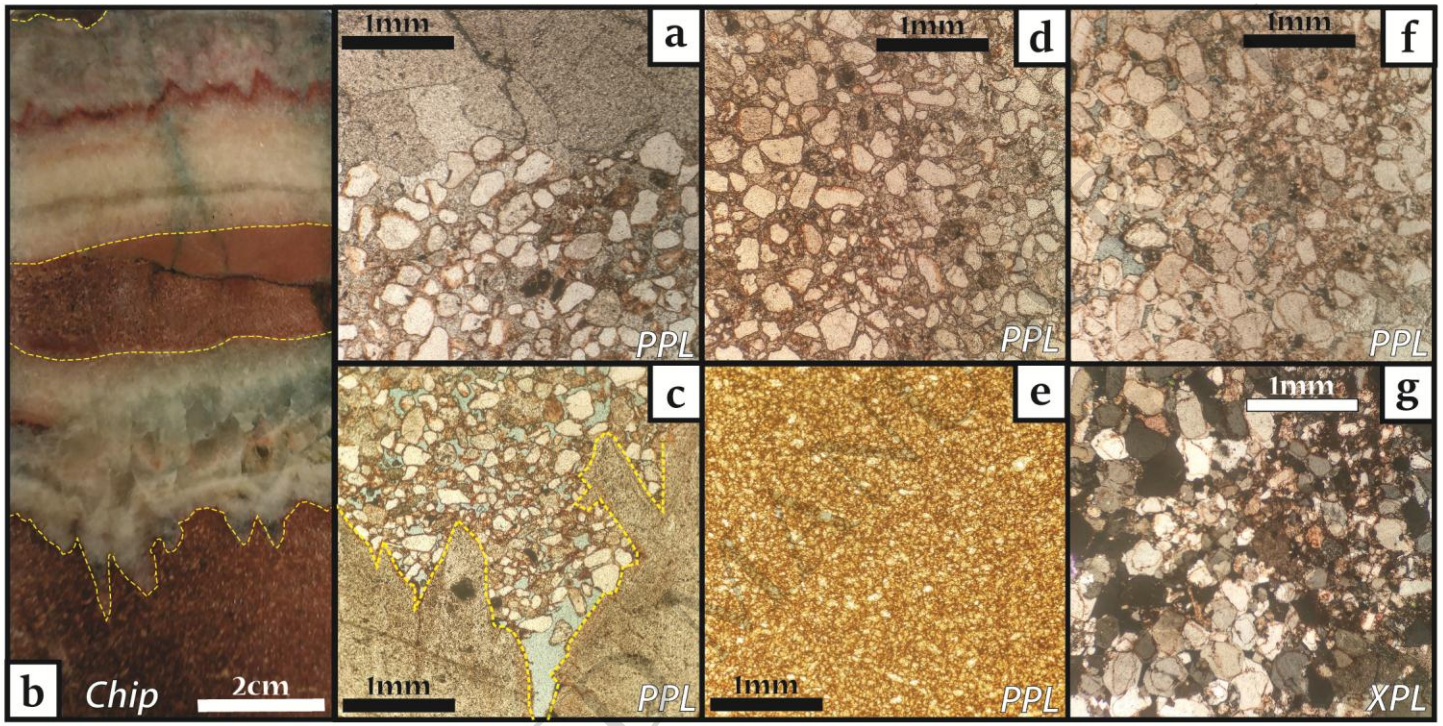

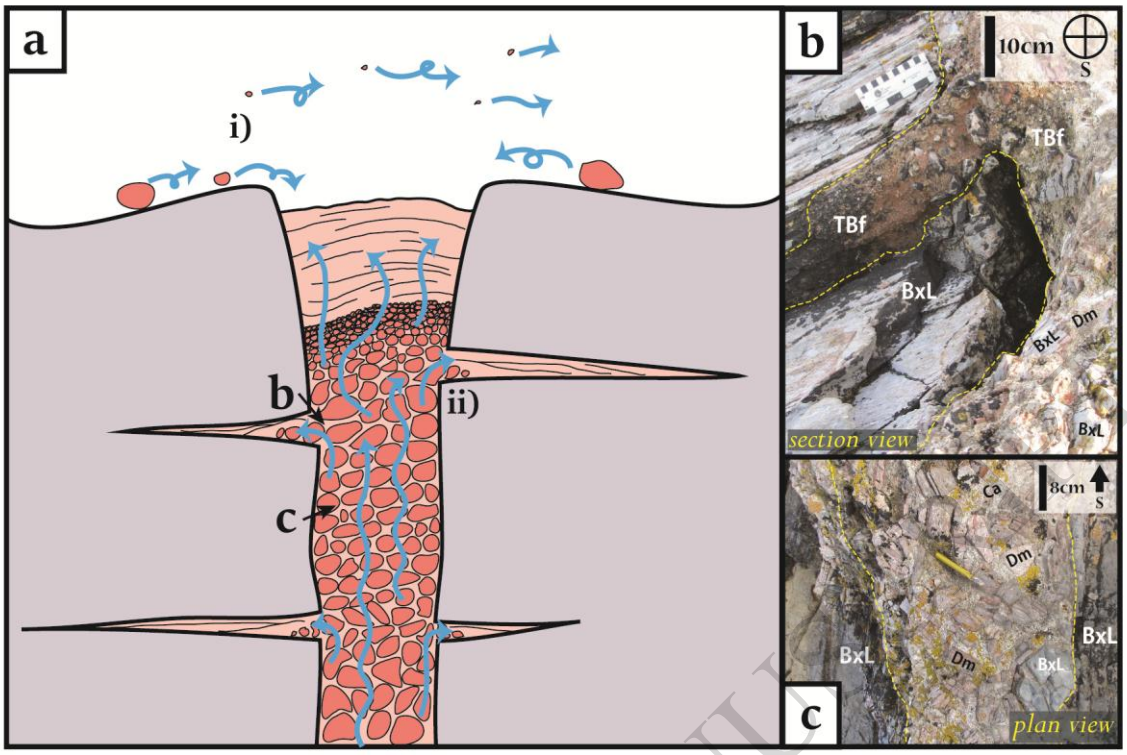

Method	σ^1	σ^2	σ^3	R	Tensor Type
R. Dihedron (Angellier, 1977)	315/85	065/02	156/05	0.22	NNE-SSW pure/radial extension
PBT Axes	355/01	230/02	140/09	0.13	NNE-SSW radial extension